Journal of Porphyrins and Phthalocyanines
J. Porphyrins Phthalocyanines 2012; **16**: 713–740
DOI: 10.1142/S1088424612300054

Published at http://www.worldscinet.com/jpp/

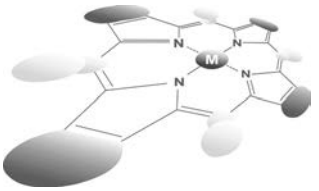

Carbon nanotubes and metalloporphyrins and metallophthalocyanines-based materials for electroanalysis

José H. Zagal*[a], Sophie Griveau[b-e], Mireya Santander-Nelli[a], Silvia Gutierrez Granados[f] and Fethi Bedioui*[b-e◊]

[a] *Universidad de Santiago de Chile, Departamento de Quimica de los Materiales, Facultad de Quimica y Biologia, Casilla 40, Correo 33, Santiago 9170022, Chile*
[b] *Chimie ParisTech, Unité de Pharmacologie Chimique et Génétique et Imagerie, 11 rue Pierre et Marie Curie, 75005 Paris, France*
[c] *CNRS, UMR 8151, 75005 Paris, France*
[d] *Université Paris Descartes, 75006 Paris, France*
[e] *INSERM, U1022, 75005 Paris, France*
[f] *Universidad de Guanajuato, División de Ciencias Naturales y Exactas, Departamento de Química, Guanajuato, Mexico*

Dedicated to Professor Tebello Nyokong on the occasion of her 60th birthday

Received 13 January 2012
Accepted 16 April 2012

ABSTRACT: We discuss here the state of the art on hybrid materials made from single (SWCNT) or multi (MWCNT) walled carbon nanotubes and MN_4 complexes such as metalloporphyrins and metallophthalocyanines. The hybrid materials have been characterized by several methods such as cyclic voltammetry (CV), scanning electron microscopy (SEM), transmission electron microscopy (TEM), X-ray photoelectron spectroscopy (XPS), atomic force microscopy (AFM) and scanning electrochemical microscropy (SECM). The materials are employed for electrocatalysis of reactions such as oxygen and hydrogen peroxide reduction, nitric oxide oxidation, oxidation of thiols and other pollutants.

KEYWORDS: metallophthalocyanines, metalloporphyrins, carbon nanotubes, SWCNT, MWCNT, electroanalysis, electrocatalysis.

INTRODUCTION

Carbon nanotubes (CNTs) were discovered in 1952 by Radushkevich and Lukyanovich [1], but their discovery went unnoticed by Western scientists since their work was published in Russian language. These authors published clear images of 50 nanometer diameter tubes made of carbon. Again, in 1978 Wiles and Abrahamson [2] observed the formation of carbon fibers with diameters ranging from 4 nm to 100 nm which were indeed carbon nanotubes, but the term "carbon nanotube" was unknown at that time. So, in spite of these earlier findings, most authors attribute the discovery of carbon nanotubes to a much later paper published by Iijima [3] in 1991. After Iijima's publication, a myriad of works have been published on the subject due to the multiple applications of these materials in many areas of science and technology. Indeed, CNTs are an exceptional class of nanomaterials possessing properties such as high surface area and electrical conductivity, significant mechanical strength and good chemical stability [4–12]. Figure 1 illustrates the structure of the honeycomb basal plane graphite sheet and the formation of single-walled carbon nanotubes (SWCNTs) by folding these graphite sheets along different lattice vectors (Fig. 1a). Folding

◊SPP full member in good standing

*Correspondence to: José H. Zagal, email: jose.zagal@usach.cl; Fethi Bedioui, email: fethi-bedioui@chimie-paristech.fr, tel: +33 144-27-64-92, fax: +33 144-27-64-96

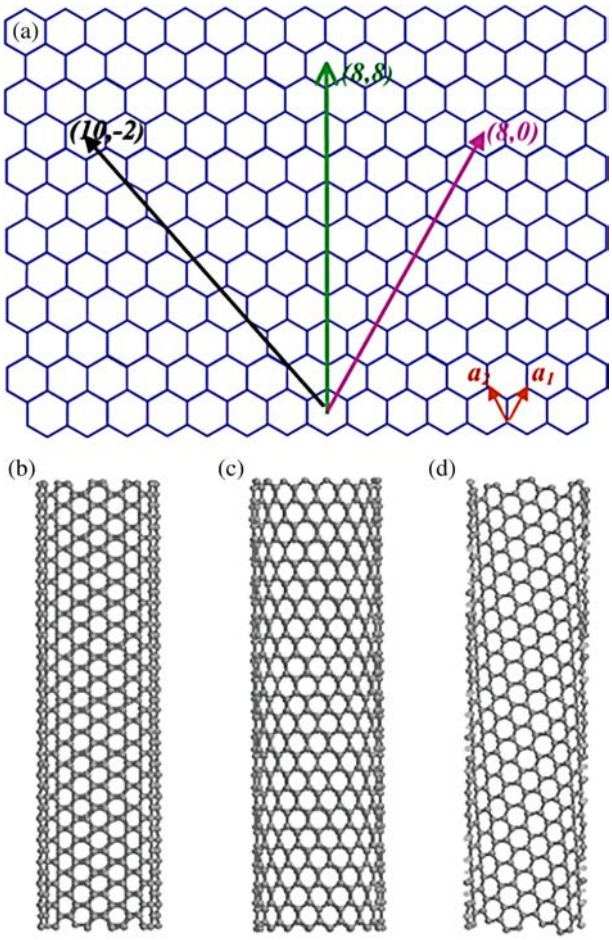

Fig. 1. (a) Structure of the honeycomb basal plane graphite sheet. Single-walled carbon nanotubes (SWCNTs) can be formed by folding the graphite sheet along different lattice vectors. Folding of (8,8), (8,0) and (10-2) vectors give armchair (b) zig-zag (c) and chiral (d) tubes; adapted from [5]

of (8,8), (8,0) and (10-2) vectors give armchair (Fig. 1b) zig-zag (Fig. 1c) and chiral (Fig. 1d) single-walled and multiwalled carbon nanotubes (MWCNTs), respectively [5]. Their vast applications include photovoltaics [13, 14], optoelectronics [15], sensors [16–18], hydrogen storage materials [19, 20], supports for electrocatalysts for fuel cell electrodes [21–35], materials for low temperature superconductors [36], artificial muscles [37] and immobilization of enzymes and nucleic acids [38–40]. These are few examples of the ever expanding field of potential applications.

In electrochemistry, CNTs are finding many applications as they exhibit a high geometrical surface area [41–43] and catalytic activity for many electron transfer reactions, when confined on electrode surfaces. Although the electrocatalytic reactivity of CNTs seems to be associated to the edge-plane-like sites or to metal impurities associated with their synthesis [44–46], it was shown by Pillay and Ozoemena that this was always the case [47]. Britto *et al*. [48] were the first to use CNT-based electrode as an electrochemical sensor, particularly for dopamine, and research has continued ever since on the application of both MWCNT and SWCNT for electrode modification, and keeps expanding into many areas. Electrode modification with CNTs was usually achieved *via* drop-dry [49] using glassy carbon electrodes (GC) or by abrasive immobilization (mainly with pyrrolytic graphite electrodes) [50, 51]. Such electrodes have been modified further with chemical [52, 53] and bioactive materials such as enzymes [49, 54–69].

On the other hand, macrocyclic metal complexes such as metalloporphyrins MPs, metallophthalocyanines MPcs and related compounds are well-known as electron transfer mediators for a great variety of reactions [70–77]. Taking advantage of the fact that MPs and MPcs adsorb strongly on graphite and carbon-based electrode materials, the possibility of using CNT to prepare *hybrid* CNT-MPc materials for electrocatalysis purposes was explored. This has resulted in the combined use of CNTs with porphyrins, phthalocyanines and heme containing enzymes and the most significant examples have been reviewed two years ago [78]. The purpose of this manuscript is to update this review of CNTs modified with metal N_4 macrocyclics, mainly porphyrins and phthalocyanines, designed for electrocatalysis or electroanalysis. More precisely, this review is built in such way that it reports first on the significant examples of methods of preparation of metal phthalocyanine or metallo porphyrin combined with CNTs and then provides major applications of these hybrid electrode materials in the field of the electrocatalytic activation of oxygen and hydrogen peroxyde reduction and the oxidation of thiols, nitric oxide, hydrazine and other biologically or environmentally releavant molecules.

METHODS OF PREPARATION OF PHTHALOCYANINE/CNT OR PORPHYRIN/CNT MATERIALS

There is a great variety of methods for obtaining electrodes containing CNT and metal N_4 macrocyclics, MN_4, including direct adsorption, functionalization and more sophisticated procedures. Figure 2 shows the structures of some of the complexes used in combination with CNTs and discussed in this paper. The MN_4 complexes are denoted as M-**x**, where M represents the central metal and **x** the number identifying the structure.

For example, Yang *et al.* [79] have reported the preparation of **Cu(II)-9** phthalocyanine covalently linked to MWCNT (**Cu(II)-9**/MWCNT) by a chemical functionalization method. The **Cu(II)-9**/MWCNT hybrid materials exhibit good solution storage stability and a low aggregation tendency due to the chemical bonding between MWCNT and asymmetrically substituted phthalocyanines. The preparation process is illustrated in Fig. 3. The same group has also reported the preparation

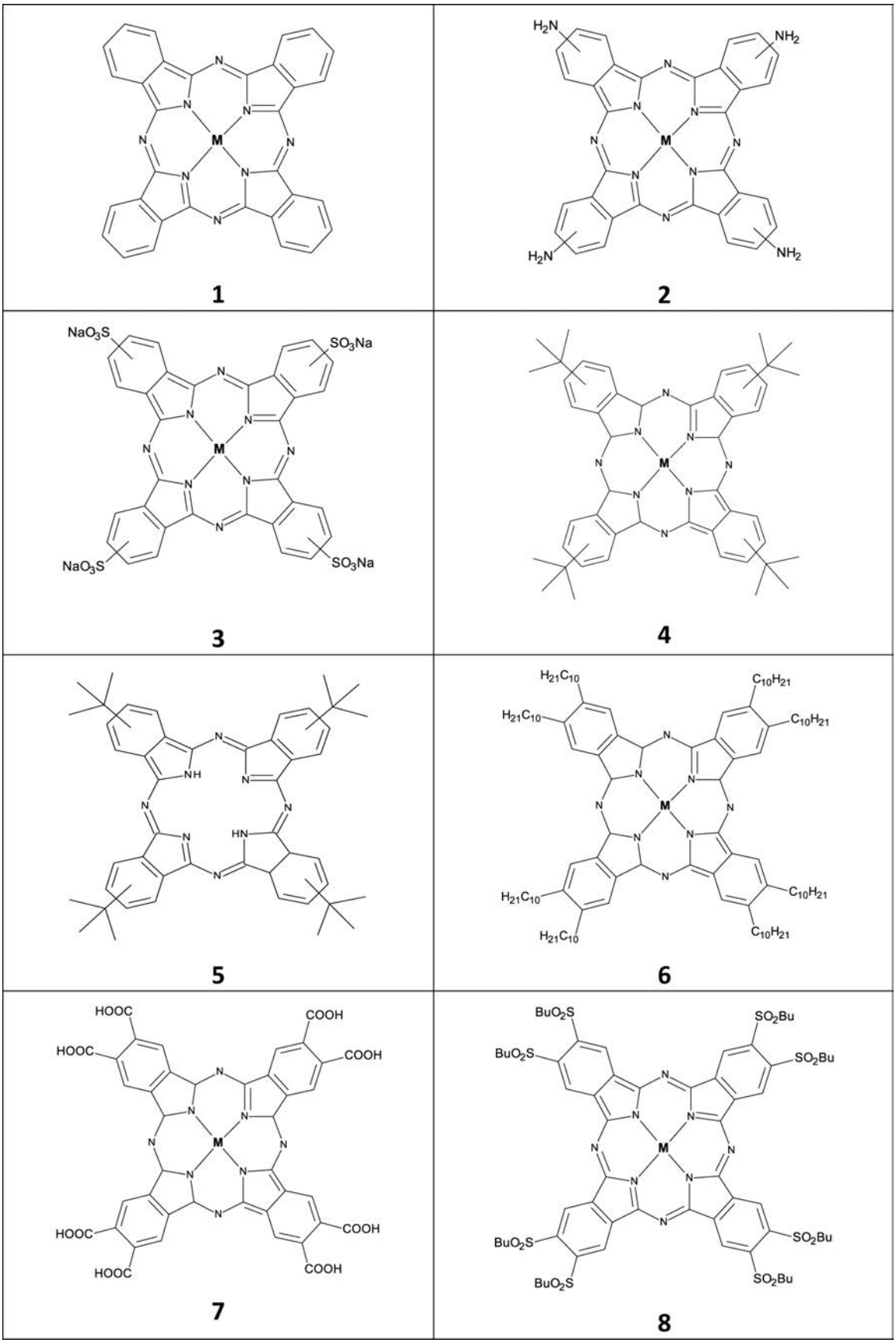

Fig. 2. Molecular structure of metallophthalocyanines and metalloporhyrins discussed in this review

of MWCNT bonded by **Mn(III)-2** [80]. The modification of the MWCNT was carried out as follows:

$$\text{MWCNT} \xrightarrow[\text{Sonicate}]{H_2SO_4/HNO_3} \text{MWCNT-COOH} \xrightarrow[\text{pyridine}]{SOCl_2} \text{MWCNT-COCl} \xrightarrow[\text{pyridine, DMF}]{\textbf{Mn(III)-2}} \text{MWCNT-}\textbf{Mn(III)-2}$$

Mugadza and Nyokong [81] adopted a similar approach to covalently link **Ni(II)-2** to carboxylic acid functionalized SWCNT as shown in Fig. 4. More recently, Chidawanyika and Nyokong [82] have reported the functionalization of SWCNTs with amine groups using a previously developed diazonium approach. This

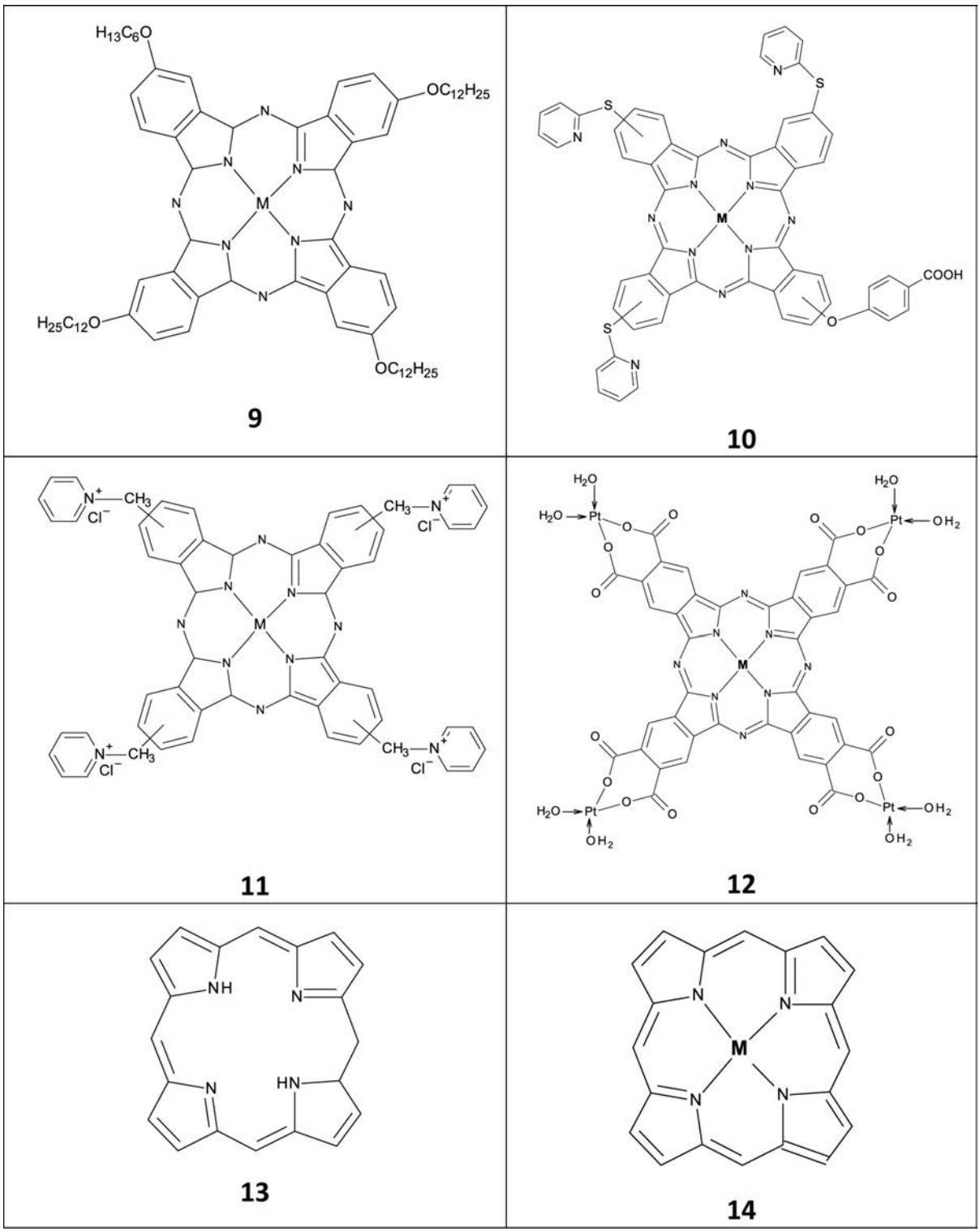

Fig. 2. (*Continued*)

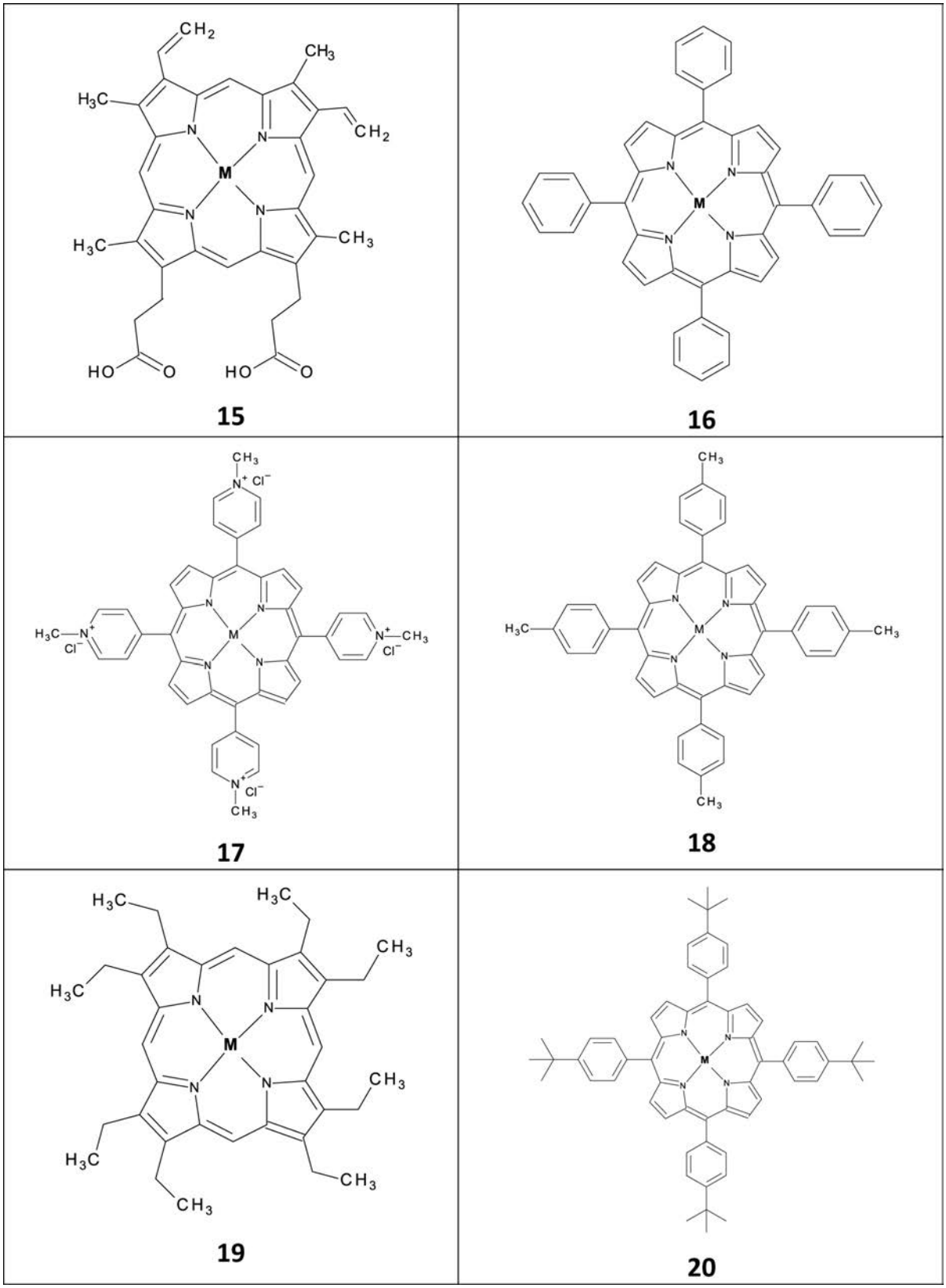

Fig. 2. (*Continued*)

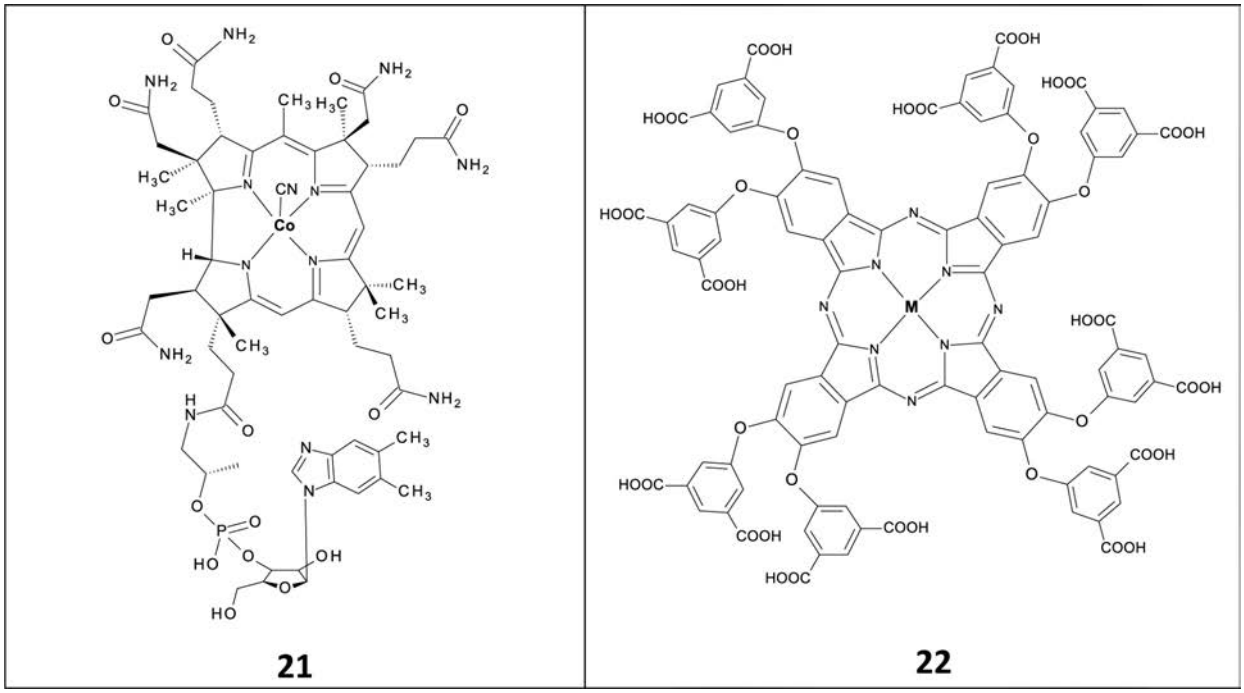

Fig. 2. (*Continued*)

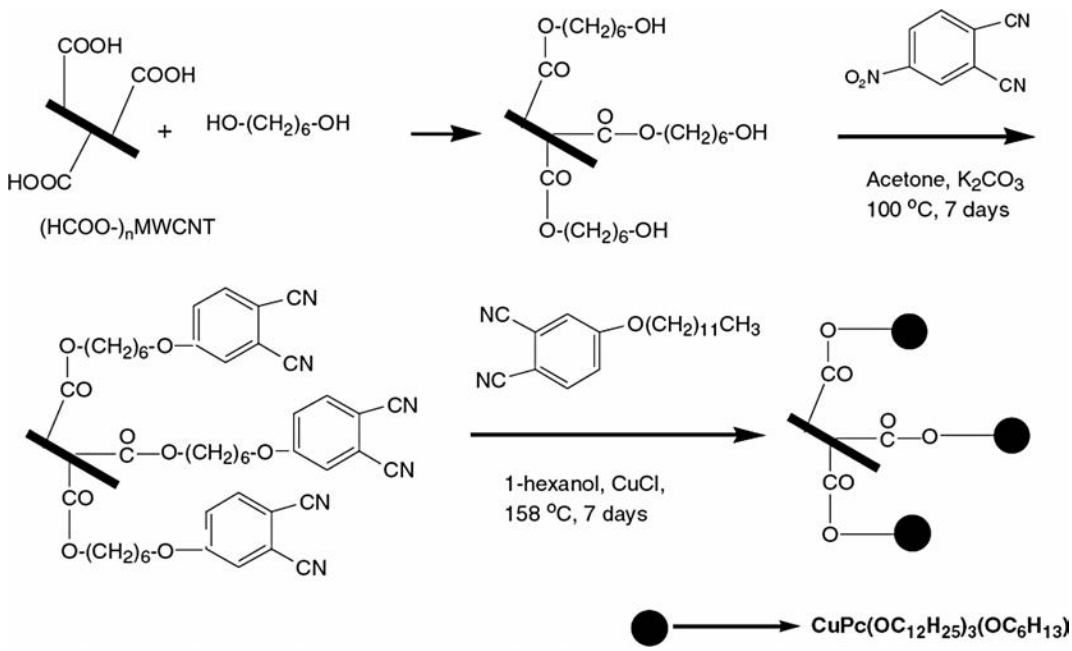

Fig. 3. Preparation of **Cu(II)-9** hybrid materials; adapted from [79]

allows the direct attachment of the **Zn(II)-10** by an amide bond as described in Fig. 5. By the same time, Baba *et al.* [83] have proposed an interesting method of preparing SWCNT/MPc hybrid ultrathin multilayers using a layer-by-layer (LBL) self-assembly approach. To achieve this, single-walled carbon nanotubes were solubilized by water-soluble cationic **Cu(II)-11** and anionic **Cu(II)-3**. The electrostatic interaction between the species was used to obtain layer-by-layer multilayers as described in Fig. 6. Highly dispersed composites were obtained due to the π–π interactions. *In situ* surface plasmon resonance spectroscopy during the layer-by-layer multilayer fabrication indicated a stepwise increase in reactivity, indicating the successive formation of nanostructured hybrid ultrathin films. Electrochemical measurements revealed that, as expected, the electrochemical response

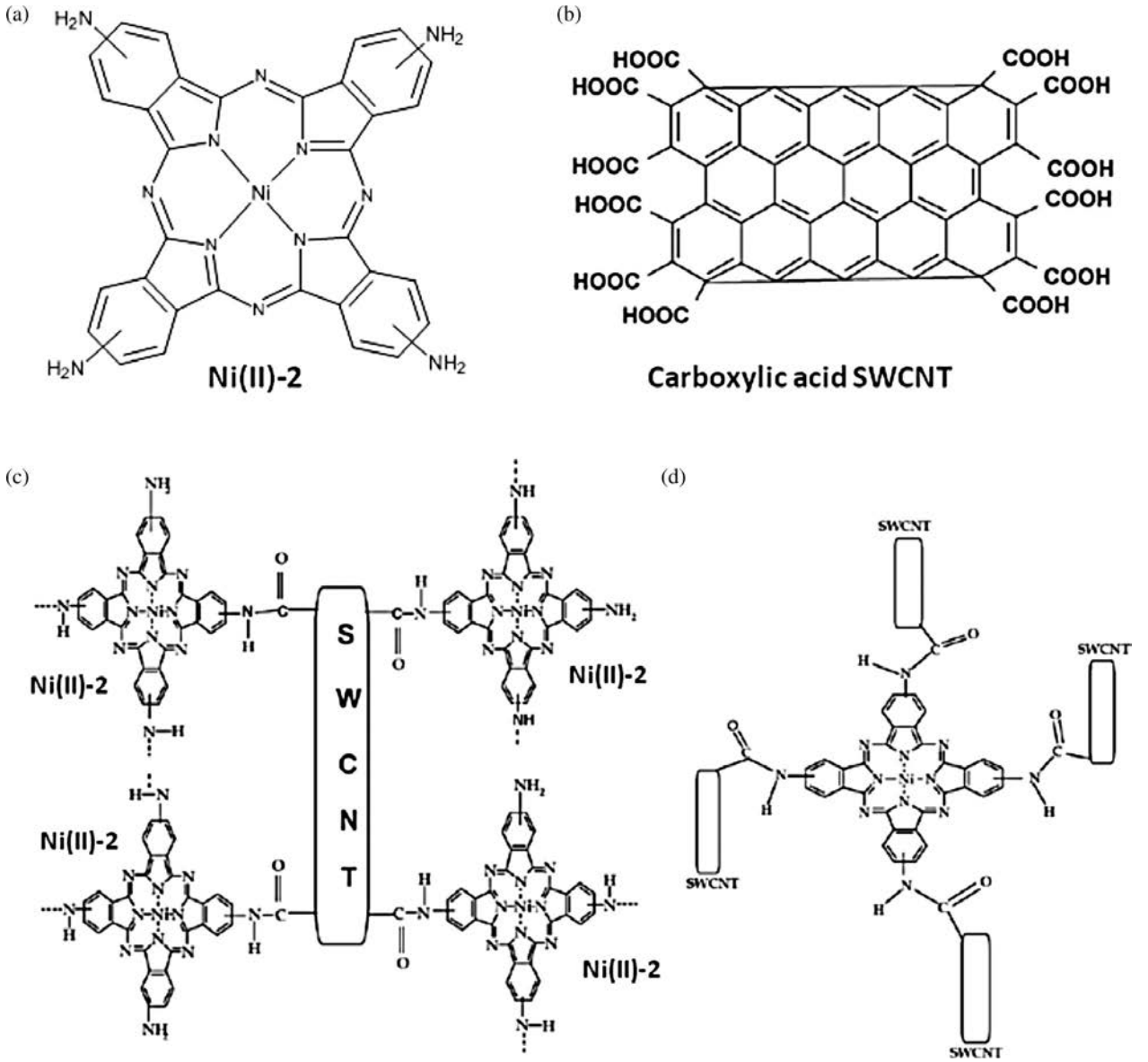

Fig. 4. Covalent grafting of **Ni(II)-2** on carboxylic acid CNT; adapted from [81]

is enhanced by the incorporation of single-walled nanotubes. Also, Ozoemena *et al.* [84] reported on the electrochemically assisted deposition of **Co(II)-3** on MWCNT as illustrated in Fig. 7.

In the case of unsubstituted N_4 complexes, they are non-covalently adsorbed onto CNTs *via* π–π interactions. Figure 8 illustrates an artists' view of porphyrins attached onto a SWCNT [85]. For example, Wang *et al.* [86] have reported that it is possible to immobilize phthalocyanine **5** on SWCNT. Immobilization is achieved by π–π interaction instead of covalent interaction, between the SWCNT and the conjugated phthalocyanine **5**. These authors report that the CNTs fade the color of the tetra-tertbutyl phthalocyanine solution in chloroform. They observed that a threshold exists for adsorption of phthalocyanine **5**, depending on the weight ratio of **5** to CNTs introduced in the solution. This method is attractive because it can be extended to other phthalocyanine macrocycles. The attachment is very strong since treatment of the modified nanotubes with different solvents under sonication and heating up to 40 °C does not remove the anchored molecules. Ye *et al.* [87] use the direct adsorption of **Fe(II)-1** from its solution onto a GCE coated with MWCNT, in order to device a glucose biosensor. In all cases, attaching CNT directly to GCE is difficult and sometimes irreproducible, therefore the use of basal plane pyrolytic graphite (BPPG) or edge plane pyrolytic graphite (EPPG) are preferred due to the inherent ability of these substrates to interact with CNTs *via* π–π interactions.

Langa *et al.* [15] have pointed out that the major drawbacks of SWCNT is that they tend to agglomerate into ropes or bundles due to strong van der Waals forces leading to poor solubility in most common solvents.

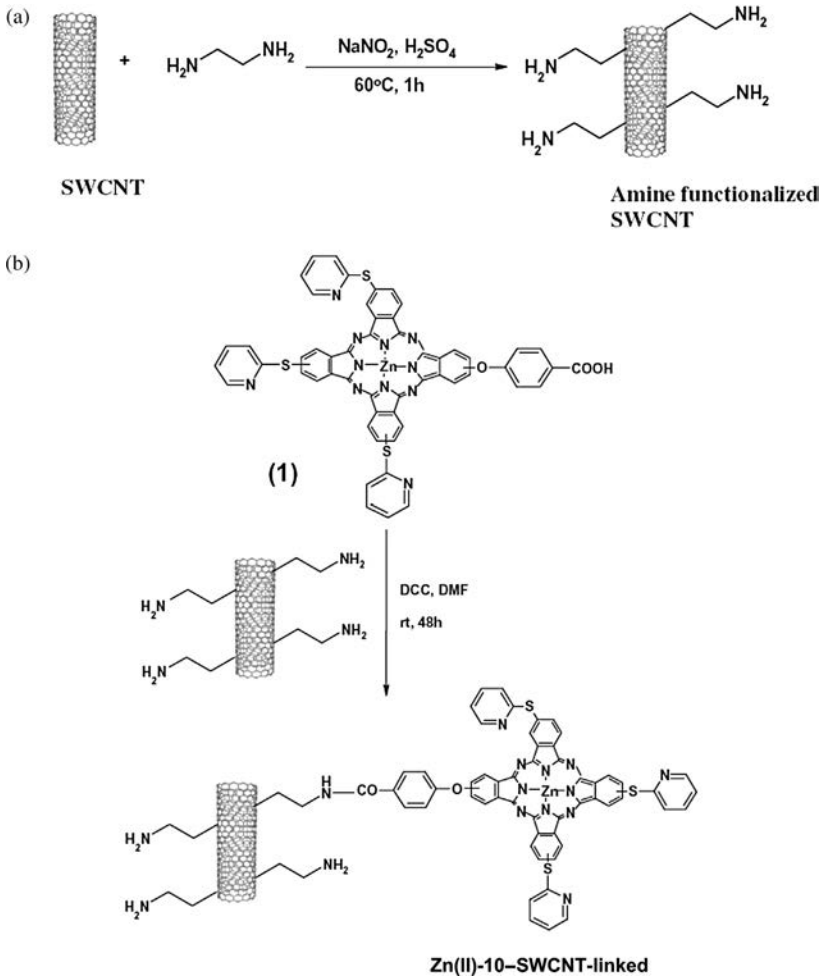

Fig. 5. Synthesis route for (a) an amine-functionalized SWCNT and, (b) **Zn(II)-10** chemically linked to SWCNT (**Zn(II)-10**–SWCNT-linked); adapted from [82]

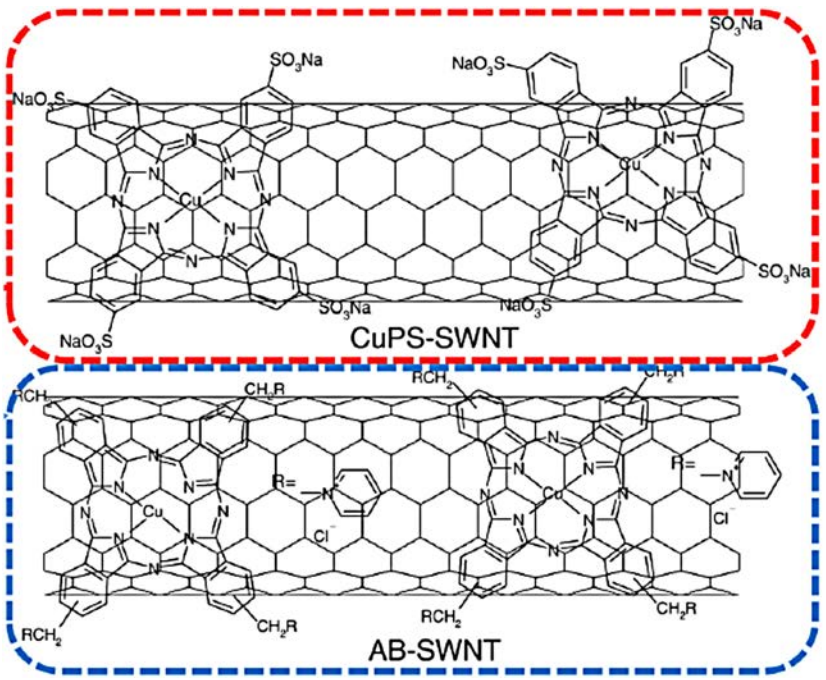

Fig. 6. Schematic drawing of the fabrication of nanostructured alcian blue pyridine variant (AB)/SWCNT/**Cu(II)-3**/SWCNT LbL films; adapted from [83]

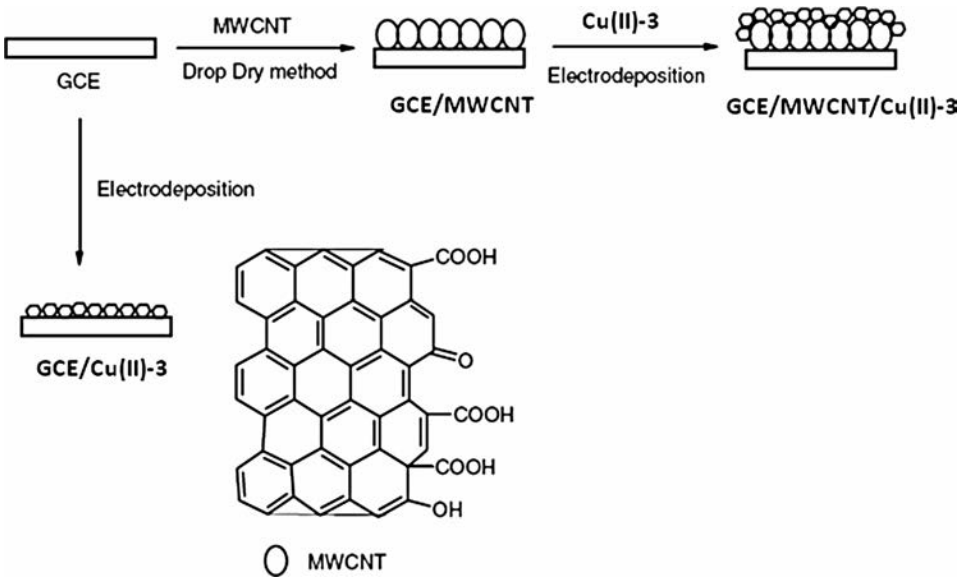

Fig. 7. Schematic procedure of electroassisted deposition of **Cu(II)-3** on MWCNT; adapted from [84]

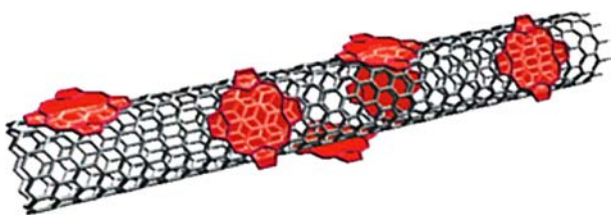

Fig. 8. Illustration of the idea of modifying a single-walled carbon nanotube with a macrocylic complex like a metalloporphyrin; adapted from [85]

Figure 9 shows an artistic picture of how porphyrin **13** provide a convenient way to build ordered molecular assemblies between porphyrins and CNTs [15, 84]. In the case of metalloporphyrins, Hasobe *et al.* [88] have reported on SWCNT-driven aggregation of porphyrin **13** to give supramolecular assemblies. Murakami *et al.* [89] have also reported the feasibility of preparation of **Zn(II)-14**-carbon nanotubes nanocomposites by dissolution of SWCNTs in a **Zn(II)-14** solution in DMF, attributed to the physical adsorption of porphyrin molecules onto the nanotube sidewall.

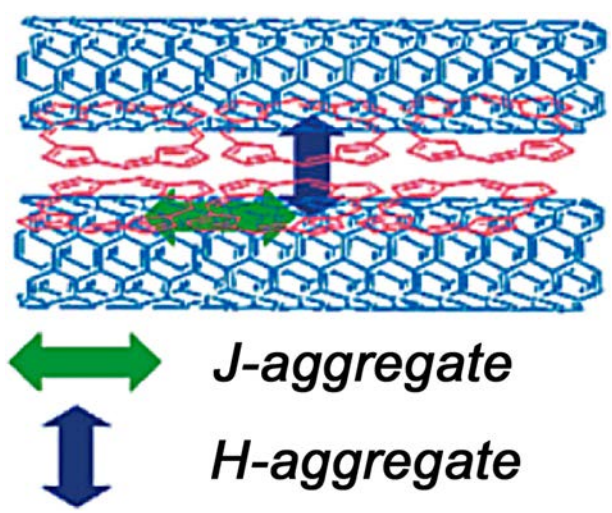

Fig. 9. Supramolecular assemblies of porphyrin molecules and SWCNT; adapted from [88]

The techniques of choice for characterizing the chemical modification of CNTs on their association with the N_4 complexes are AFM, STM and SEM. Figure 10 shows some significant (and non-exhaustive) examples of images reported in the literature. They show how these techniques bring clear views of the materials but without gaining deep insights into their chemical characterization.

ELECTROCHEMICAL CHARACTERIZATION OF CNT/METAL PHTHALOCYANINE ELECTRODES

Electrochemical behavior of the modified CNT/MPc electrodes is usually examined with a known reversible system, for example using ferricyanide, $Fe(CN)_6^{3-}$, as a redox probe. Figure 11 shows cyclic voltammograms of MWCNT/BPPG (a), *poly*-**Co(II)-2**/MWCNT/BPPG (b), *poly*-**Co(II)-2**/BPPG (c) and bare BPPG (d) recorded in a solution of 0.05 M KCl containing 1 mM $K_3[Fe(CN)_6]$ [90]. The MWCNT/BPPG and *poly*-**Co(II)-2**/MWCNT/BPPG showed approximately similar current responses. This result confirms that the attachment of the **Co(II)-2** onto the MWCNT does not adversely affect the electronic properties of the MWCNT, in agreement with previous literature work [86]. Whereas the peak separations for $Fe(CN)_6^{3-}/Fe(CN)_6^{4-}$ on BPPG and *poly*-**Co(II)-2**–BPPG are 0.147 V and 0.117 V, respectively, these decrease

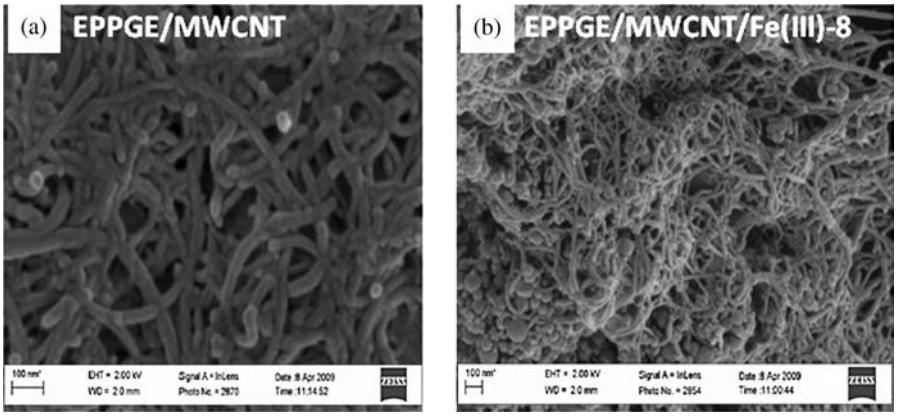

Fig. 10 A. Comparative SEM images of (a) EPPGE/MWCNT and (b) EPPGE/MWCNT/**Fe(III)-8**; adapted from [93]

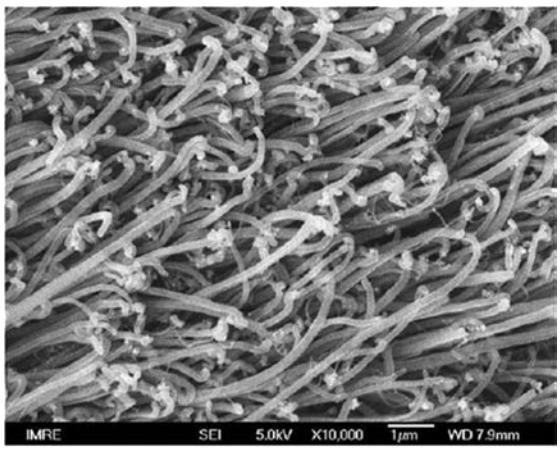

Fig. 10 B. SEM images of well-aligned MWCNTs; adapted from [105]

to 0.097 V for both the MWCNT–BPPG and the *poly*-**Co(II)-2**–MWCNT–BPPG. Hence, the rate of electron transfer at the electrode surface is improved with the attachment of MWCNTs and **Co(II)-2**-MWCNT compared to the BPPG surface. The peak labeled (I) in Fig. 11 appears only in the presence of **Co(II)-2**. This peak is thus associated with the oxidation of **Co(II)-2**. This peak is most likely due to Co^{III}/Co^{II} process, since the first oxidation in cobalt phthalocyanine complexes occurs at the central metal. This process has been observed near 0.5 V (*vs.* Ag|AgCl) on GC for poly-**Co(II)-2** [85], thus, as expected, the potential of the peak can depend on the electrode employed. It should be noted that the Co^{III}/Co^{II} process is known to be irreversible for adsorbed **Co(II)-2** complexes at neutral pH values and shows very poor voltammetric features [91].

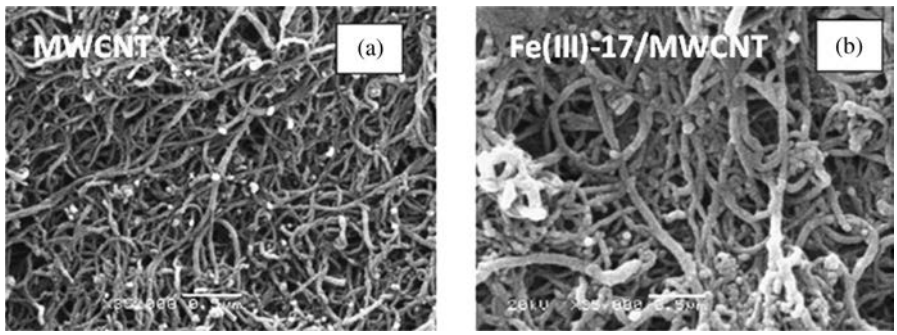

Fig. 10 C. SEM images of (a) MWCNT and (b) **Fe(III)-17**/MWCNT; adapted from [120]

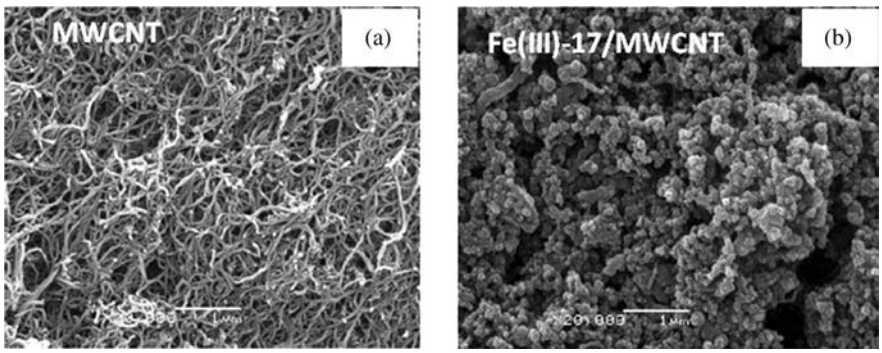

Fig. 10 D. SEM images of (a) MWCNT and (b) **Fe(III)-17**/MWCNT; adapted from [121]

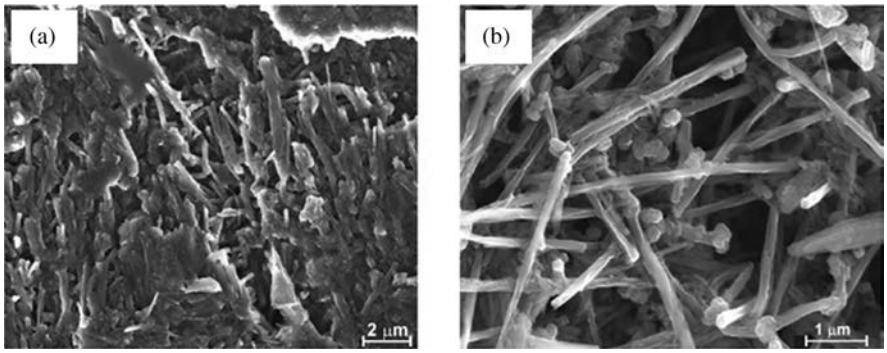

Fig. 10 E. FEG-SEM micrographs for parrafin/MWCNT/**Co(II)-1** composite Electrode (a): magnitude of 10 K×; (b) magnitude of 80 K×; adapted from [144]

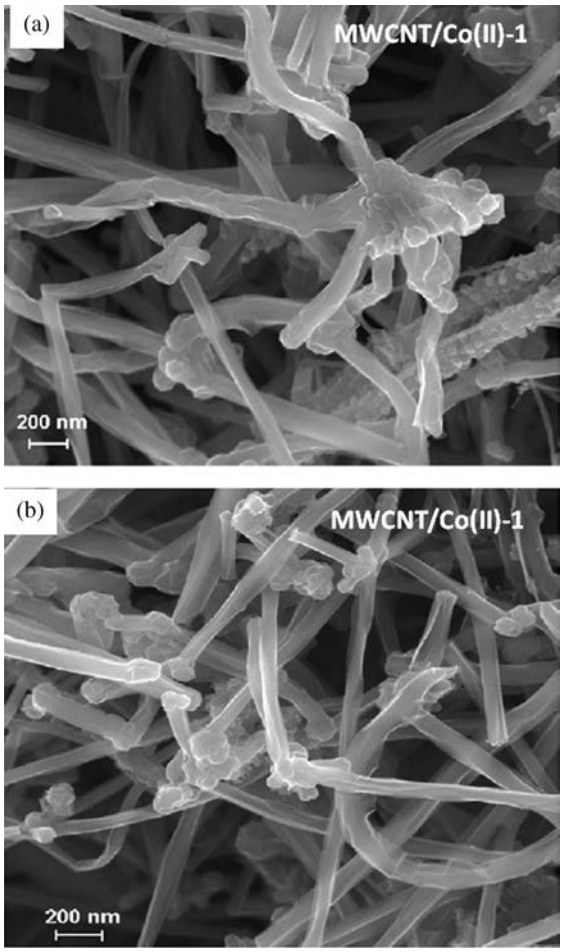

Fig. 10 F. FEG-SEM micrographs for (a) MWCNT and (b) MWCNT/**Co(II)-1**; adapted from [145]

Murakami *et al.* [85] have characterized dispersion of raw (r-SWCNT) and purified (p-SWCNT) CNTs modified with **Fe(III)-15** and **Fe(III)-16** complexes. Transmission electron and atomic force microscopy, as well as UV-visible near IR spectroscopies showed that the **Fe(III)-15** derivatives individually dissolved the p-SWCNTs in polar solvents. These authors characterized the p-SWCNT/**Fe(III)-15** cast films on GC and a typical cyclic voltammogram is illustrated in Fig. 12, where the cast p-SWCNT/**Fe(III)-15** on GC is compared to the response of the **Fe(III)-15** adsorbed directly on GC. At both electrodes the redox couple corresponding to the Fe(III)/(II) process is observed at -0.12 V *vs.* SCE. The amount of redox active sites is 3.2×10^{-10} mol.cm^{-2} for adsorbed **Fe(III)-15**, whereas it is 6.5×10^{-10} mol. cm^{-2} for p-SWCNT/**Fe(III)-15**. These differences can be attributed to changes in the apparent surface area in presence of the CNTs.

Cyclic voltammetric and electrochemical impedance spectroscopy EIS data revealed that the electrosorbed **Co(II)-2** is highly stable and well organized, with an electron-transfer rate constant in ferricyanide solution (of 6×10^{-5} cm.s^{-1}) comparable to that of the SWNCT [92]. The preferential electrosorption process was attributed to strong π-stacking interactions between **Co(II)-2** and the side-walls of the SWCNTs, with possible synergistic covalent interactions. EIS was also used to characterize CNT electrodes modified with **Co(II)-8** and **Fe(III)-8** [93]. Modified Randles equivalent electrical circuits were developed to fit the data. The electrolyte resistance, electron transfer resistance, constant phase element, double layer capacitance and Warburg-type impedance, associated with the diffusion of the ions of the redox probe were used as fitting parameters. The apparent heterogeneous electron transfer rate constants were then estimated. According to the results, the authors conclude that the modified electrodes are constant phase elements.

Silva *et al.* [94] performed one of the rare characterizations of CNT/MPc electrode using scanning electrochemical microscopy SECM. The obtained results allowed confirming that adsorbed **Co(II)-1** does not block the electrochemical activity of the nanotubes. Although information obtained from SECM should not be over-emphasized, they still provide clear evidence for electrode functionalized by SWCNT/**Co(II)-1** with higher electron exchange rate properties**.**

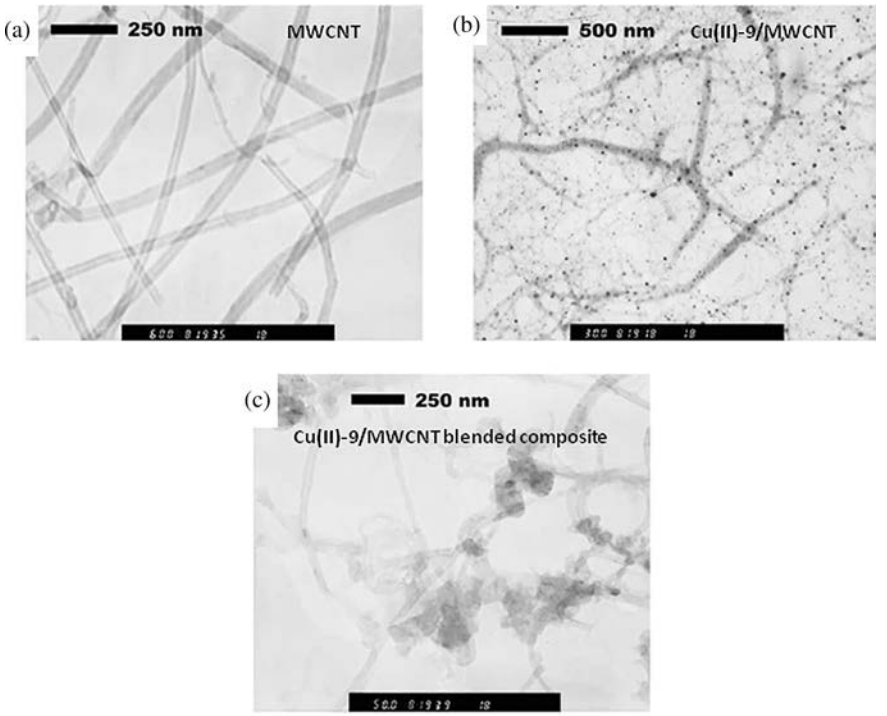

Fig. 10 G. TEM images of (a) MWCNT, (b) **Cu(II)-9**–MWCNT hybrid materials and (c) **Cu(II)-9**/MWCNT blended composite (9:1, by wt.); adapted from [79]

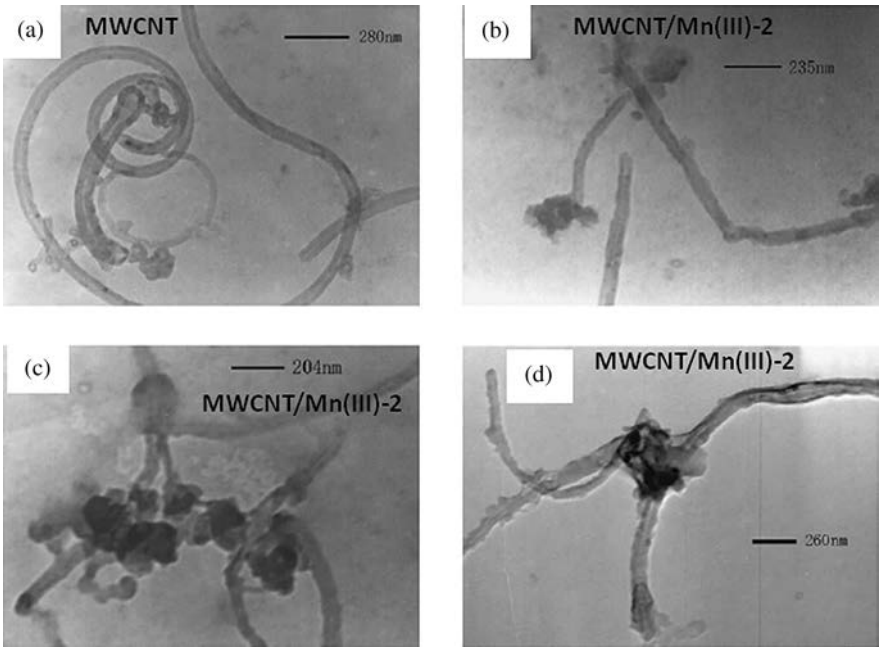

Fig. 10 H. TEM images of MWCNT (a), and MWCNT/**Mn(III)-2** (b)–(d); adapted from [80]

ELECTROCATALYTIC AND ELECTROANALYTIC APPLICATIONS

Oxygen reduction reaction (ORR)

The catalytic activity of metallophthalocyanines and MN_4 macrocyclic complexes for the ORR is well-known [70, 95, 96]. On the other hand, carbon and graphite materials in general are modest catalysts for the ORR [96, 97] in alkaline media and their small activity is linked to surface defects present on the electrode. Further, they only catalyze the 2-electron reduction to peroxide. However the simple modification of these electrodes with CNTs increases their catalytic activity for the reaction

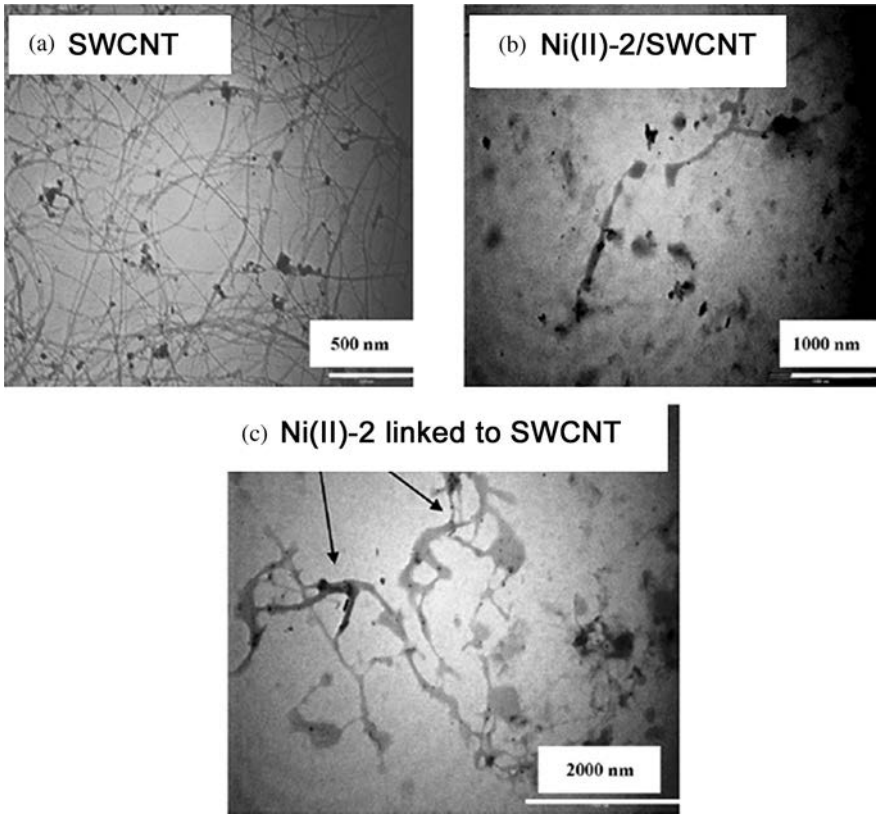

Fig. 10 I. TEM images of (a) functionnalized SWCNT; (b) **Ni(II)-2**/SWCNT and **Ni(II)-2** linked to SWCNT; adapted from [81]

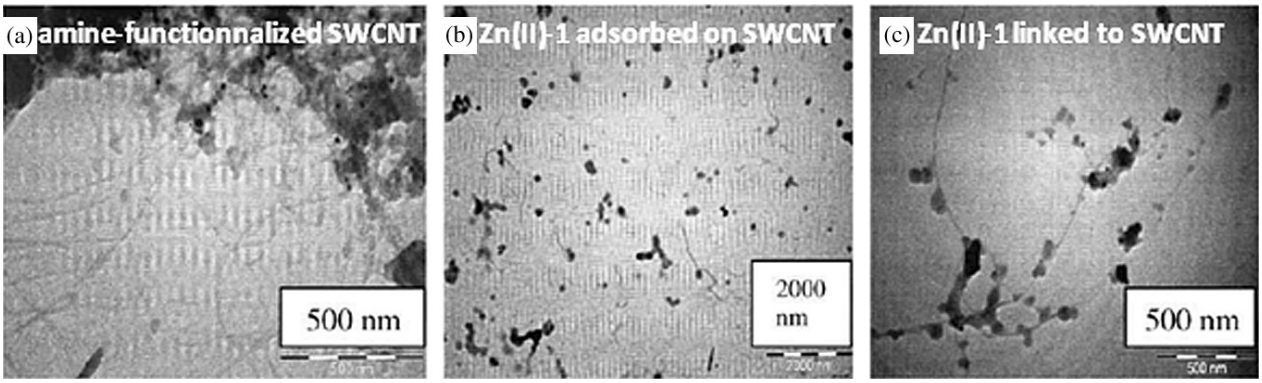

Fig. 10 J. TEM images of (a) amine-functionnalized SWCNT; (b) **Zn(II)-1** adsorbed on SWCNT; (c) **Zn(II)-1** linked to SWCNT; adapted from [82]

but does not change the reaction pathway (*i.e.* 2-electrons involved). The increase in activity is due to two main factors: an increase in real surface area and an increase in the amount of surface defects that are present on the external walls or at the edges or carbon nanotubes. This has been discussed in detail in reviews by Compton *et al*. [45] and Banks *et al*. [46]. Along these lines Qu *et al*. [99] have found that the activity of glassy carbon increases upon modification with MWCNT for the reduction of oxygen in buffer solution (pH 3.8). As expected, modification of GC by adsorption of **Co(II)-14** on the MWCNTs, increases the catalytic activity for O_2 reduction even further. They observe a shift in the reduction peak potential of O_2 by 0.12 V (*vs.* Ag|AgCl) compared to the electrode with no cobalt porphyrins and also an increase in the current. Electrochemical experiments show a total number of electrons transferred for oxygen reduction of about 3. This suggests that two parallel processes take place *via* 2 electrons and 4 electrons for reduction of oxygen to give peroxide and water respectively. Meanwhile, the catalytic activities of the multilayer film (MWCNTs/**Co(II)-17**)(n) prepared by layer-by-layer method were investigated and the results showed that the peak current for O_2 reduction increased and the peak potential shifted in the positive

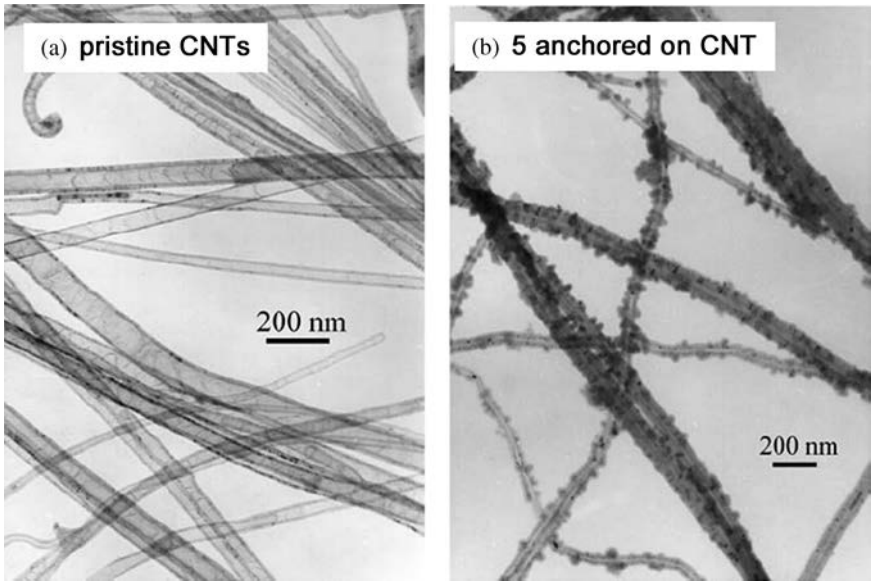

Fig. 10 K. (a) TEM image of pristine CNTs, (b) typical TEM image of **5** densely anchored on CNT surfaces after treatment; adapted from [86]

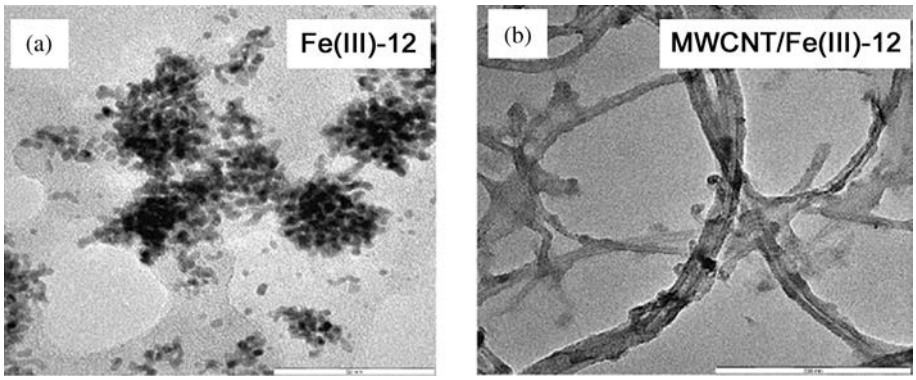

Fig. 10 L. TEM images of (a) **Fe(III)-12** and (b) MWCNT/**Fe(III)-12**; adapted from [100]

direction with the increase of the number of layers. The catalytic properties in alkaline solution of **Fe(II)-12** catalyst supported on MWCNTs for the ORR were studied by Ozoemena and Mamuru [100]. For complexes bearing an iron center, a direct 4-electron transfer process is observed. It is not clear however if the Pt atoms located on the periphery of the phthalocyanine ligand contribute to the catalytic currents.

Schuhmann *et al*. [101] studied the electrocatalytic reduction of oxygen at electropolymerized films of **Mn(III)-18**, **Fe(III)-18** and **Co(II)-15** supported on MWCNTs. They pre-stabilized the MWCNTs with ultra-thin layers of organic 4-(pyrrole-1-yl) benzoic acid. These authors point out the importance of the multiple oxidation states of manganese as central metal ion as potential advantages for the electron transfer process during the ORR in a 0.1 M phosphate buffer solution. Electropolymerization of metal porphyrins produces catalytically active films. The incorporation of MWCNTs in the film decreases the amount of hydrogen peroxide produced during the ORR and induces a significant positive shift of the oxygen reduction potential. Of the complexes studied, **Mn(III)-18** showed the highest catalytic activity and stability for oxygen reduction. Figure 13 illustrates the considerable effect in the voltammetric response for ORR when CNT are incorporated into the system for tetratolyl metalloporphyrin. The same group [102] used SECM with the redox competition mode to visualize the local electrocatalytic activity of metalloporphyrin spots for ORR in 0.1 M phosphate buffer. The metalloporphyrin spots were obtained by electrochemically induced deposition using a droplet cell. **Mn(III)-18**, **Fe(III)-18** and **Co(II)-18** have been investigated, and the authors found the Mn complex to show the highest catalytic activity. The RC-SECM revealed that when using **Mn(III)-18** modified electrode the lowest amount of H_2O_2 was formed compared to **Fe(III)-18** and **Co(II)-18**. This clearly indicates that O_2

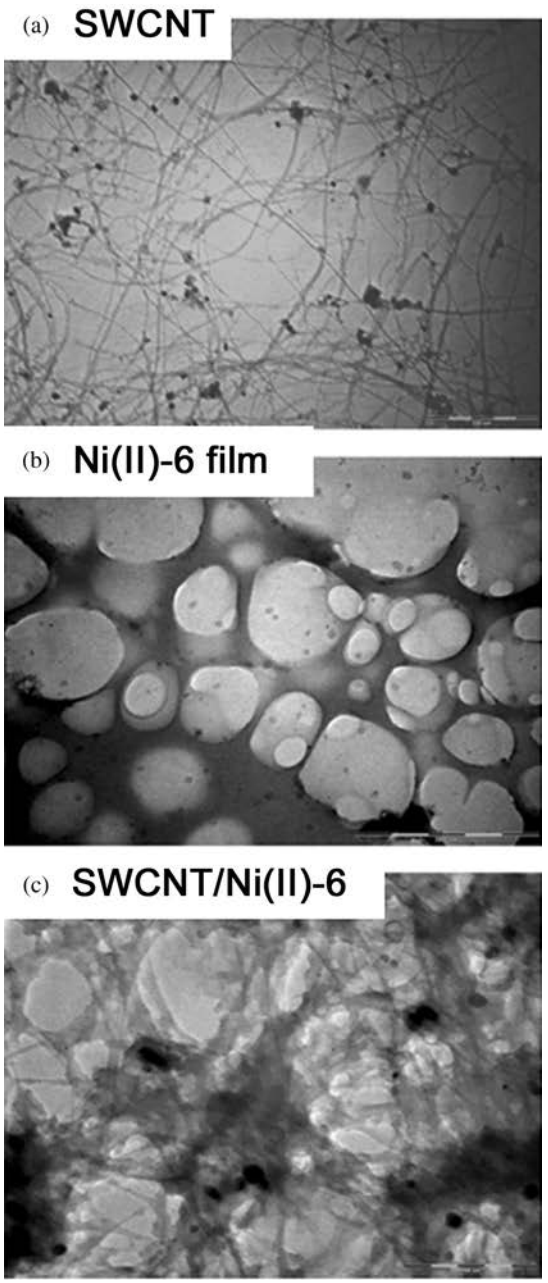

Fig. 10 M. TEM images of SWCNT (a), **Ni(II)-6** film (b) and SWCNT/**Ni(II)-6** (c); adapted from [142]

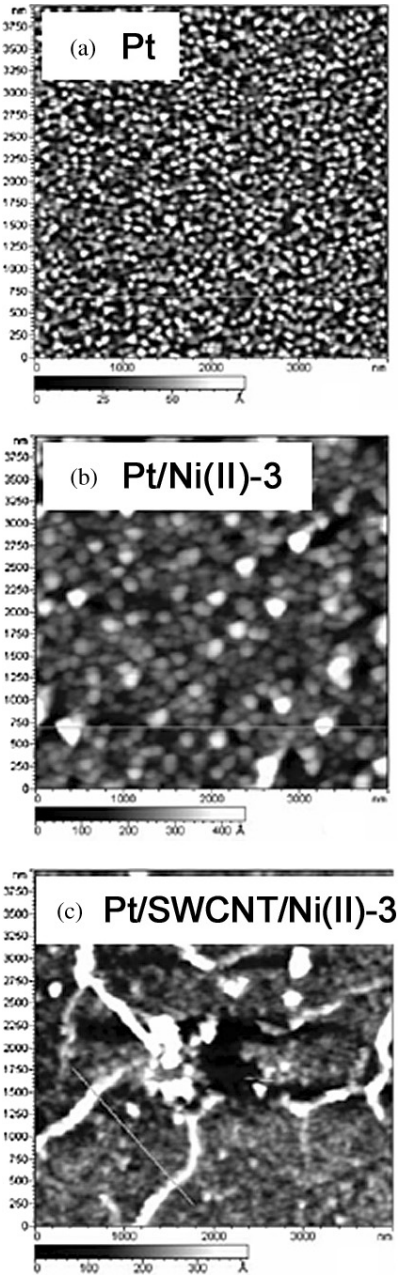

Fig. 10 N. Tapping mode AFM images of (a) bare Pt, (b) Pt/**Ni(II)-3**, and (c) Pt/SWCNT/**Ni(II)-3** electrode surfaces; adapted from [139]

reduction for the Mn complex proceeds almost entirely *via* 4 electrons. This was confirmed using rotating ring-disk measurements.

A recent report [103] describes the use of a ruthenium phthalocyanine deposited on MWCNT that promotes the direct ORR to water *via* 4 electrons. The authors use a ruthenium phthalocyanine based catalyst **Ru(II)-12** supported on MWCNT electrode and tested the activity by rotating disk electrode voltammetry. Zhan *et al*. [104] reported that positively charged heme proteins assembled with SWCNT into layer by layer films on solid surfaces gave stable composite electrodes with good electrocatalytic properties towards ORR. Along the same lines, Ye *et al.* [105] have reported that a **Fe(III)-15**-modified MWCNT electrode can be obtained by simple adsorption of **Fe(III)-15** on well-aligned MWCNT. Cyclic voltammetry of the **Fe(III)-15**-modified MWCNT electrode in pH 7.4 phosphate buffer solution clearly shows the dioxygen reduction peak close to 0 V *vs.* Ag/AgCl (Fig. 14). These results are useful in the development of a novel oxygen sensor for working at a relatively low potential.

Qu *et al.* [99] have reported that combining Pt nanoparticles and cobalt porphyrin co-produce highly

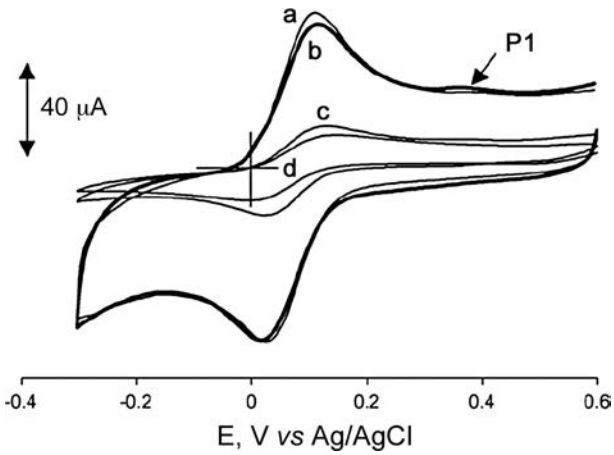

Fig. 11. Cyclic voltammograms of (a) MWCNT/BPPGE, (b) poly-**Co(II)-2**/MWCNT–BPPG, (c) poly-**Co(II)-2**/BPPG, and (d) BPPG in 10^{-3} M $K_3[Fe(CN)_6]$. The peak labeled as P1 is observed only in presence of **Co(II)-2**. Scan rate = 25 mV/s; adapted from [90]

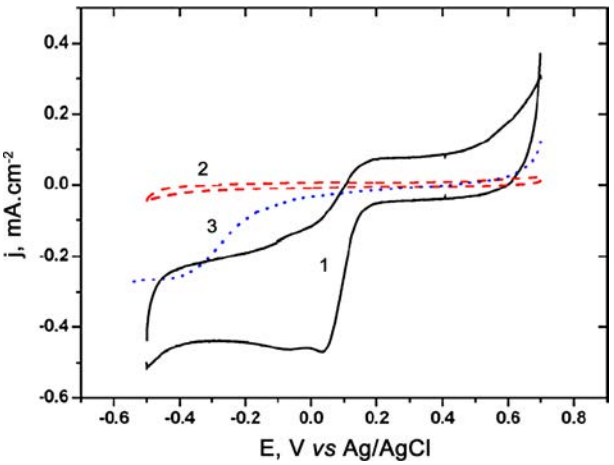

Fig. 13. Cyclic voltammograms for the reduction of oxygen (in O_2 in saturated phosphate buffer (0.1 M), pH 7) catalyzed by electropolymerized **Mn(III)-18** on (1) MWCNT support and (3) bare glassy carbon. Curve (2) shows the background response of curve (3) in de-aerated electrolyte; adapted from [101]

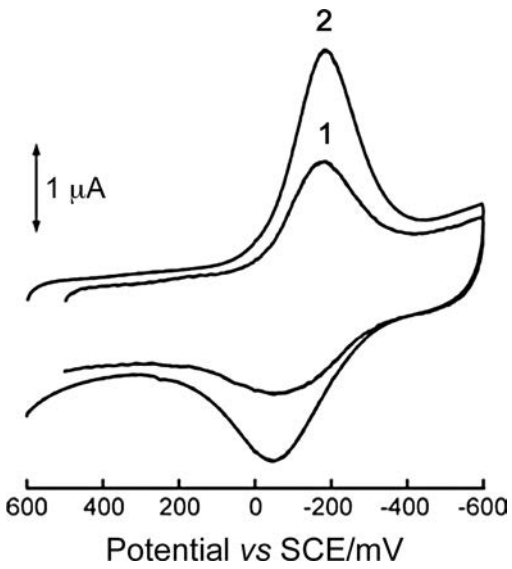

Fig. 12. Cyclic voltammograms of cast films of **Fe(III)-15** (1) and p-SWCNTs/**Fe(III)-15** (2) on glassy carbon electrodes mixed in an aqueous solution of a 0.1 M $HClO_4$ and 0.1 M $NaClO_4$. Potential scan rate 0.1 V/s; adapted from [85]

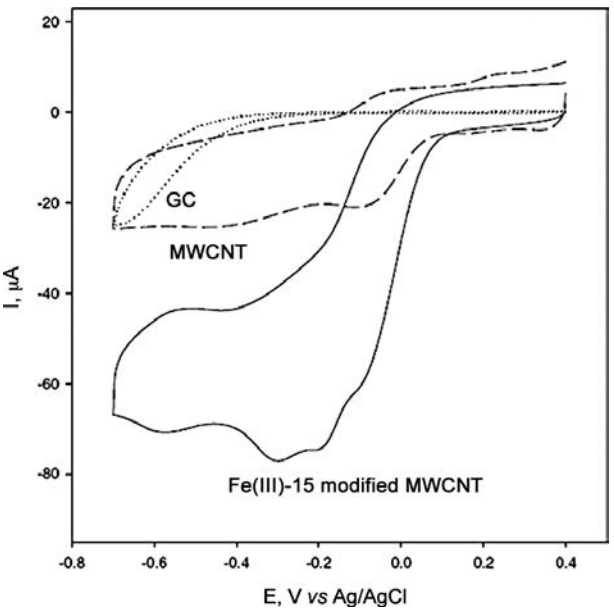

Fig. 14. Cyclic voltammogram of a GC electrode (dotted line), bare MWCNT/GC electrode (dashed line) or **Fe(III)-15** modified MWCNT/GC electrode (solid line) in electrolyte saturated with O_2. Phosphate buffer solution pH = 7.4; adapted from [105]

active electrodes for ORR. To achieve this, they prepared a hybrid thin film containing Pt nanoparticles and **Co(II)-17** modified MWCNT (MWCNT/**Co(II)-17**/$PtCl_6$) on GC electrode. To prepare the composite electrode, the first step consisted in making a GC/MWCNT modified electrode by evaporating a solution of previously purified MWCNTs in ethanol. The GC/MWCNTs electrode was then immersed in a 1 mM **Co(II)-17** solution and, at last, was put in a K_2PtCl_6 solution. In this way the $PtCl_6^{2-}$ anion was adsorbed on the GC/MWCNT/**Co(II)-17** electrode by electrostatic interaction. Reduction of the GC/MWCNT/**Co(II)-17**/$PtCl_6^{2-}$ was achieved by polarizing the modified electrode at -0.7 V *vs.* Ag|AgCl. The presence of Pt(0) upon reduction of the film was verified by XPS. Figure 15 illustrates tapping mode AFM images of the modified electrode before and after reduction. Before reduction, only some bundle like structures are observed. After reduction the Pt nanoparticles can be clearly distinguished, having diameters ranging from 120 to 200 nm. The particles are inserted to the inner wall of the CNTs. Multilayered electrodes were obtained by repeating the procedures described before. The films

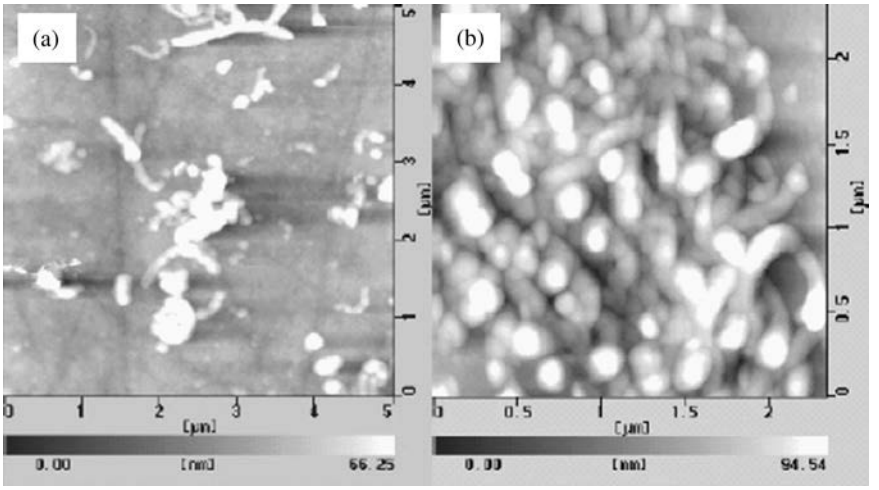

Fig. 15. AFM images (a) MWNT/**Co(II)-17**/PtCl6 film assembled on a GC electrode before electrochemical reduction, (b) MWNT/**Co(II)-17**/Pt after electrochemical reduction at -0.7 V *vs.* Ag/AgCl under anaerobic conditions; adapted from [99]

obtained are very stable over days in contact with air. The GC/MWCNT/**Co(II)-17**/Pt modified electrode shows high catalytic activity for the reduction of O_2 *via* 4 electrons to give H_2O. It is not clear from this paper what the role of **Co(II)-17** is in the overall catalytic process since electrodes without Pt show less activity. However it is a good starting point for efficient catalyst for potential applications in fuel cells.

Even though not necessarily using carbon nanotubes but carbon nanofibers, Maldonado *et al.* [106] have reported a facile method for the direct preparation of carbon nanofiber (CNF) electrodes by pyrolysis of iron phthalocyanine on nickel substrates. Uniform, large area coverage is observed with aligned bundles of CNFs exhibiting bamboo-like, hollow fibril morphology possessing diameters of 40–60 nm and the length of approximately 10 μm. The electrochemical behavior and stability of CNF electrodes as oxygen reduction catalysts were investigated by electrochemical methods. Without an extensive electrode pretreatment or surface activation, these electrodes exhibit significant electrocatalytic activity in aqueous KNO_3 solutions at neutral to basic pH for the reduction of dioxygen to hydrogen peroxide. As determined from chronocoulometry, the overall electrochemical reaction proceeds by the peroxide pathway *via* two successive one-electron reductions. pH-dependent cyclic voltammetry studies indicate that the CNF electrodes are very active toward adsorption. At pH < 10, the one-electron reduction of O_2 to superoxide is rate limiting, whereas at more alkaline pH the reduction process is limited by the protonation of adsorbed superoxide. XPS, Raman, and TEM measurements suggest that the disorder in the graphite fibers and the presence of exposed edge plane defects and nitrogen functionalities are important factors for influencing adsorption of reactive intermediates and enhancing electrocatalysis for O_2 reduction.

Jousselme *et al.* [107] have prepared recently electrodes by modifying carbon nanotubes with several MN_4 metal macrocyclics. They have dispersed **Fe(III)-1**, **Co(II)-4**, **Co(II)-19**, and **Co(II)-20** on CNTs. Figure 16 shows an artistic view of the incorporation of the catalysts onto the CNTs. They tested different types of CNTs (SWCNTs, DWCNTs and MWCNTs) and examined the electrocatalytic activity of these systems for ORR in alkaline and acidic solutions. They found that the activity increases when increasing the number of walls in the CNTs. This is expected since multiwalled CNTs have more defects where complexes can adsorb. However, the authors assume the complexes are present on the graphene walls of the CNTs. This might not be necessarily true. The highest activity is obtained with **Fe(III)-1** and this is also not a surprising result since **Fe(III)-1** promotes the ORR *via* 4 electrons in contrasts to most N_4 macrocyclics having a Co central metal.

Reduction of H_2O_2

Turdean *et al.* [108] have reported that **Fe(III)-15**, adsorbed either on SWCNT or on hydroxyl-functionalized SWCNT (SWCNT-OH), can be incorporated within a Nafion® matrix immobilized on the surface of a graphite electrode. From cyclic voltammetric measurements, performed under different experimental conditions (pH and potential scan rate), they found that the Fe(III)/Fe(II) redox couple involves the transfer of one electron and one proton. The heterogeneous electron transfer process is faster when **Fe(III)-15** is adsorbed on SWCNT-OH (~11 s^{-1}) than on SWCNT (~4.9 s^{-1}). Both the SWCNT-**Fe(III)-15**- and SWCNT-OH-**Fe(III)-15**-modified graphite electrodes exhibit electrocatalytic activity for the reduction of H_2O_2 and of nitrite. The modified electrode sensitivities were found to vary in the following sequences: $S_{SWCNT\text{-}OH\text{-}Fe(III)\text{-}15}$ = 2.45 mA/M ≅

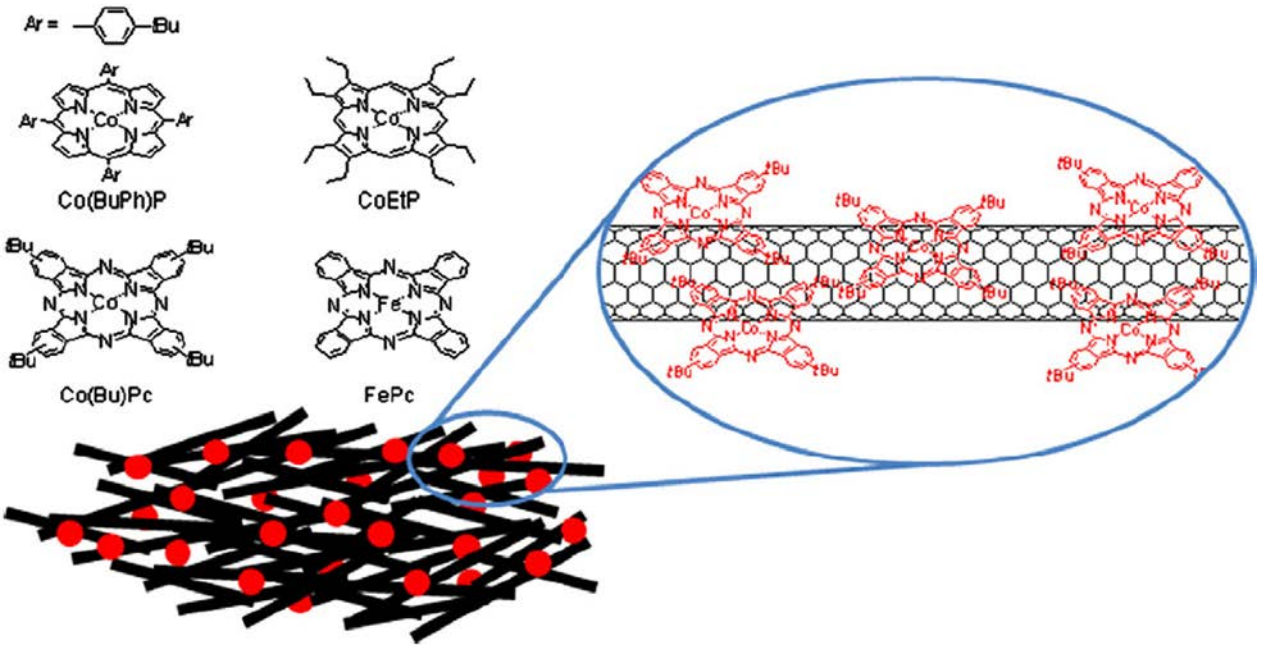

Fig. 16. Schematic representation of the hybrid catalysts formed with SWCNT and **Co(II)-4**; adapted from [107]

$S_{SWCNT\text{-}Fe(III)\text{-}15}$ = 2.95 mA/M > $S_{Fe(III)\text{-}15}$ = 1.34 mA/M for H_2O_2, and $S_{SWCNT\text{-}Fe(III)\text{-}15}$ = 3.54 mA/M > $S_{Fe(III)\text{-}15}$ = 1.44 mA/M > $S_{SWCNT\text{-}OH\text{-}Fe(III)\text{-}15}$ = 0.81 mA/M for NO_2^-.

Ozoemena and Pillay [109] have proposed a very interesting approach for the fabrication of a nanostructured platform of poly(m-aminobenzenesulfonic acid), (denoted as PABS), functionalised SWCNT and **Fe(III)-1** nanoparticles using layer-by-layer (LBL) self-assembly strategy. The authors monitored the substrate build-up, *via* strong electrostatic interaction. Figure 17 illustrates the LBL approach to achive the nano**Fe(III)-1** and SWCNT-PABS supramolecular system on a gold surface. The authors show that as the number of bilayers increases, the electron transfer kinetics of the ferricyanide/ferrocyanide redox probe decreases. However, exactly the opposite is observed for the electrochemical reduction of H_2O_2. The enhancement in the electrochemical response for H_2O_2 detection demonstrates that the LBL approach is an interesting nano-architectural sensing platform for the development of a biosensor for peroxide.

Reduction and oxidation of nitrite

Turdean *et al.* [108] reported that **Fe(III)-15**, adsorbed either on SWCNT or on hydroxyl-functionalized SWCNT (SWCNT-OH), as described above, shows catalytic activity for the reduction of nitrite and H_2O_2. Ho *et al.* [109] have reported the catalytic oxidation of nitrite on the poly(3,4-ethylenedioxythiophene)/**Fe(III)-1**/MWCNT (PEDOT/**Fe(III)-1**/MWCNT) modified screen-printed carbon electrodes (SPCE). These authors compared kinetic parameters, such as overpotential, current density and rate constant at PEDOT/**Fe(III)-1**/MWCNT-modified SPCE, with an unmodified screen printed carbon electrode (SPCE), with SPCE/**Fe(III)-1** and with SPCE/MWCNT/**Fe(III)-1** for the electro-oxidation of nitrite. Taking as reference the unmodified SPCE, they observed an increase in the anodic peak current density and a decrease in the anodic peak potential of 0.150 V for electro-oxidation of nitrite when the electrode was modified with FePc. After introducing an under-layer of MWCNT onto the **Fe(III)-1**-modified SPCE, labeled as **Fe(III)-1**/MWCNT-modified SPCE, the heterogeneous electron transfer rate constant at **Fe(III)-1**/MWCNT-modified SPCE increased by about 7.8 times as compared to that of the **Fe(III)-1**-modified SPCE. The current response could increase even further after depositing a layer of PEDOT film on the **Fe(III)-1**/MWCNT-modified SPCE, labeled as PEDOT/**Fe(III)-1**/MWCNT-modified SPCE. This effect was concomitant with a decrease in the oxidation peak potential. The authors attributed the effect of the PEDOT to a pre-concentration effect induced by the electrostatic interaction between the negatively charged nitrite and oxidized PEDOT film. As an overall effect, the PEDOT/**Fe(III)-1**/MWCNT-modified SPCE reduces the overpotential for the oxidation of nitrite by *ca.* 0.330 V with an enhancement of the currents by a factor of 3.5 times compared with unmodified SPCE. The sensitivity and limit of detection (S/N = 3) for the PEDOT/**Fe(III)-1**/MWCNT-modified SPCE were 638 $mA.cm^{-2}.M^{-1}$ and 71 nM, respectively. The sensor was tested satisfactorily for the determination of nitrite in tap water samples.

Oxidation of thiol and other pollutants

The catalytic activity of metallophthalocyanines for the oxidation of thiols is well documented [70, 72, 73,

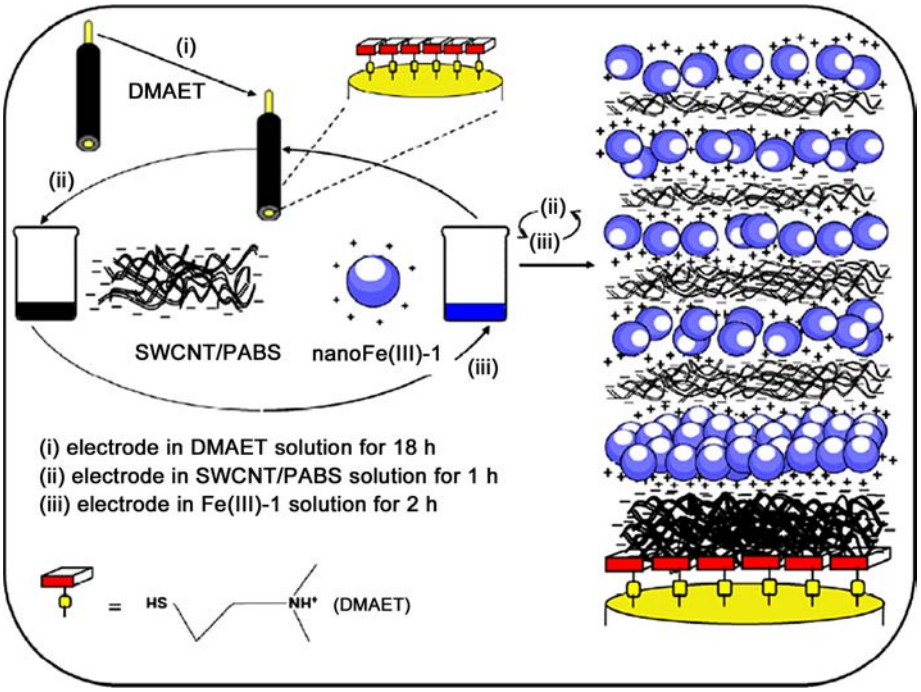

Fig. 17. Schematic representation depicting the layer-by-layer assembly of nanoFe(III)-1 and SWCNT-PABS on gold surface (this representation is not drawn to scale); adapted from [109]

109–121]. Silva *et al*. [94] reported on the electrocatalytic oxidation of thiols using carbon nanotubes. Figure 18 shows the cyclic voltammograms of 5 mM of 2-mercaptoethanol (2-ME) in 0.1 M NaOH solution on unmodified GC (curve 1), GC/**Co(II)-1** (curve 2), GC/SWCNT (curve 3) and GC/SWCNT-**Co(II)-1** (curve 4) electrodes. The bare GC and GC/SWCNT electrodes (without **Co(II)-1**) show practically no activity towards 2-ME oxidation, while the presence of **Co(II)-1** catalyses the oxidation of the thiol, as evidenced by the appearance of an anodic current (curves 2 and 4) so-called electrocatalytic current [70, 73]. The most important feature is the significantly enhanced catalytic effect induced by the combination of SWCNT and **Co(II)-1**, in terms of enhancement of the anodic current and reduction in the overpotential of the thiol oxidation process. Indeed, in the case of GC/SWCNT-**Co(II)-1** modified electrode, a neat decrease in overpotential of 2-ME oxidation is obtained (-0.15 V), relative to the response of GC/**Co(II)-1** electrode. Also, as it can be clearly seen in Fig. 18, a large enhancement of 20 fold (at E = -0.4 V) in the oxidation current is obtained at the GC/SWCNT-**Co(II)-1**, relative to the response at GC/**Co(II)-1**. This figure shows that in both cases, GC/**Co(II)-1** and GC/SWCNT-**Co(II)-1** electrodes, the appearance of the peak related to the oxidation of 2-ME is concomitant with that of a reduction peak, during the reverse scan, at about -1.1 V and -0.95 V, respectively (curves 2 and 3). This large cathodic peak is related to the reduction of the corresponding disulfide [70, 73]. From these results, it appears clearly that SWCNT-**Co(II)-1** not only acts as a very efficient catalyst towards the oxidation of 2-ME but also as a catalyst for the reduction of the corresponding disulfide with an enhanced electron transfer rate (3 fold relatively to GC/**Co(II)-1** electrode).

Voltammetric measurements were also performed under controlled convection by using rotating electrode technique. The reported data confirm that no passivation of the electrode surface upon 2-ME oxidation occurred. More importantly, they emphasize the fact that under hydrodynamic conditions, the GC/SWCNT-**Co(II)-1** electrodes are mechanically stable. This allows a possible use of this class of hybrid electrodes in flow injection analysis conditions. By the same way, Porras *et al.* [119] prepared glassy carbon electrodes modified with CNTs incorporated into a polymeric polypyrrole matrix. The polymeric matrix enables stabilization and control of the deposit formed on the surface, obtaining a good electrode material with respect to the oxidation-reduction of FeMeOH. The inclusion of **Co(II)-1** in the composite material on the electrode surface induces a catalytic effect towards the electrooxidation of 2-ME, the combination GC/CNT/PPy/**Co(II)-1** presenting the best compromise in terms of oxidation current peak intensity and of oxidation potential. These results suggest that such strategy leading to formation of composite material on electrode surface by electrochemical methods is suitable for the development of electrochemical sensors.

Luz *et al*. [120] have developed a highly sensitive voltammetric sensor for reduced L-glutathione (GSH) using a basal plane pyrolytic graphite (BPPG) electrode modified with **Fe(III)-17** adsorbed on MWCNT. The

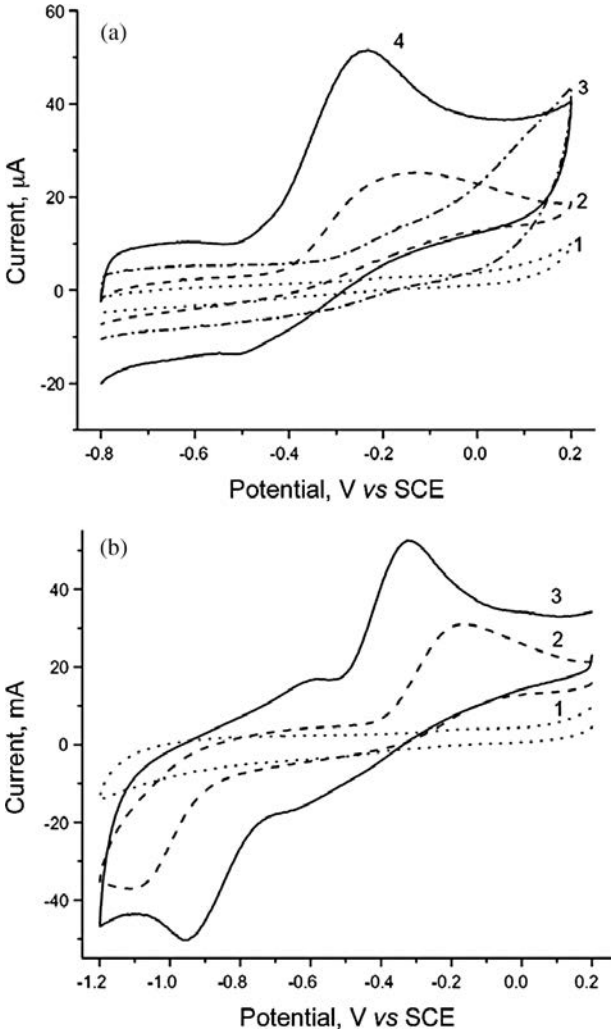

Fig. 18. Cyclic voltammograms of 2-ME (5 mM) in 0.1 M NaOH aqueous solution at different GC hybrid electrodes (a): restricted potential range. Curve 1: unmodified GC; curve 2: GC/**Co(II)-1** adsorbed electrode; curve 3: GC/SWCNT electrode and curve 4: GC/SWCNT/**Co(II)-1** electrode. (b): Extended potential range. Curve 1: unmodified GC; curve 2: GC/**Co(II)-1** adsorbed electrode; curve 3: GC/SWCNT/**Co(II)-1** electrode. Scan rate = 0.1 V/s; adapted from [94]

modified electrode exhibited high catalytic activity for L-glutathione oxidation. They obtained a linear response range from 5 μM to 5 mM with a sensitivity of 703.41 μA.mM^{-1}. The detection limit for GSH observed was 0.5 μM and the relative standard deviation for 10 determinations of 250 μM GSH was 1.4%. Later on, the same group [121] reported a similar study on the development of a supramolecular structure using two metal complexes: Co(II)-3 and **Fe(III)-17** adsorbed on MWCNT. They investigated this system for the oxidation of GSH. By using square wave voltammetry as shown in Fig. 19, they found a linear response in the range 2 to 210 mM, with a sensitivity of 1570 mA.mM^{-1}. The detection limit was found to be 0.03 μM and relative standard deviation of 110 mM GSH was 2.6%

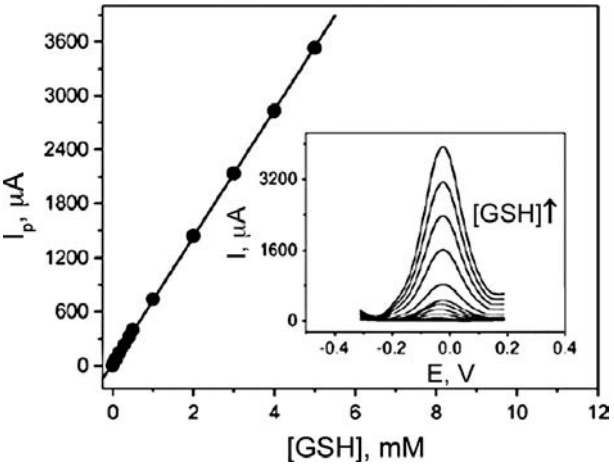

Fig. 19. Analytical curve for the electro-oxidation of GSH in phosphate buffer solution at pH 7.4 in the concentration range 0.005 to 5 mM. Step potential (E) = 0.002 V, frequence (f) = 80 Hz and amplitude (a) = 0.03 V (insert: the square wave voltammograms of the analytical curve); adapted from [120]

(n = 10). The authors tested all electrodes described above for GSH determination in erythrocyte samples and the results were in agreement to those obtained by alternative analytical methods described in the literature.

Oxidation of hydrazine

The catalytic activity of MPcs for the oxidation of hydrazine is well-known [70, 95, 122–135] Geraldo *et al*. [136] have developed a SWCNT functionalized with **Co(II)-1** which shows that the presence of the nanotubes enhances the catalytic activity of the **Co(II)-1** itself without any change in the reaction mechanism. A synergistic effect was observed in terms of reactivity when the new nanocomposite material was adsorbed on the GC electrode. The obtained hybrid electrodes were tested under hydrodynamic conditions: two different oxidation processes were observed, which suggested the presence of two different types of active sites on the electrode surface catalyzing the reaction. AFM images showed clear differences in surface roughness for each electrode confirming the different compositions of the hybrid electrodes.

Chen *et al*. [137] have prepared composite electrodes containing MWCNTs and **21** deposited on glassy carbon, gold, and indium tin oxide. The MWCNT/**21** electrodes show catalytic activity towards hydrazine oxidation. They obtained a linear calibration curve by amperometry in the hydrazine concentration range from 2.0 μM–1.95 mM for MWCNT/**21** electrodes. The sensitivity of the electrode was estimated to 1.32 mA.cm^{-2}.mM^{-1} and the detection limit to 0.7 μM.

Oxidation of nitric oxide, NO

Silva *et al.* [94] reported on the electrocatalytic oxidation of NO using SWCNT/MPc electrodes. For

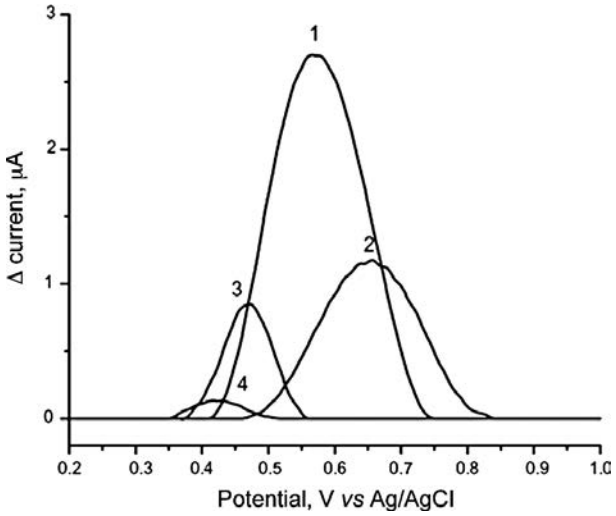

Fig. 20. Cyclic voltammetry peaks (after baseline subtraction) of 0.1 mM NO in phosphate buffer solution (pH 7.4) at different composite electrodes. Curve 1: GC/SWCNT-**Ni(II)-3**; curve 2: GC/**Ni(II)-3**; curve 3: GC/SWCNT and curve 4: unmodified GC. Note that all electrodes were cast with an outermost external layer of Nafion®. Cyclic voltammograms were recorded immediately after the addition of the NO stock solution in aerated electrochemical cell; adapted from [94]

that purpose, a SWCNT-**Ni(II)-3** hybrid GC electrode was reported. Indeed, it is known that **Ni(II)-3** adsorbed or electropolymerized onto carbon or platinum electrode allows the electrocatalytic activation of NO oxidation in aqueous solution [138]. Figure 20 shows the cyclic voltammetric peaks (obtained after subtracting the baseline current for each electrode, only the anodic scans are shown for simplicity) of 0.4 mM NO in phosphate buffer solution (pH = 7.4) recorded at different composite electrodes immediately after the addition of NO. In all cases, the electrodes were covered with Nafion® in order to avoid interfering voltammetric signals from the anodic oxidation of eventual traces of nitrite in the solution, formed upon reaction of NO with dissolved oxygen. Although the oxidation of NO occurs at GC/SWCNT and GC at lower potential values than at the **Ni(II)-3**-containing coatings, probably due to specific electrocatalytic features on these two raw materials, it can be emphasized from these data that the use of GC/SWCNT-**Ni(II)-3** allows a neat enhancement in the peak intensity related to NO oxidation (curve 1), compared to unmodified GC (curve 4) or GC/SWCNT (curve 3) composite electrodes. This again clearly indicates that the combined use of both SWCNT and **Ni(II)-3** allows the enhancement of the electrocatalytic performances for NO oxidation (curves 1 and 2) in terms of current intensity. This is an important result since the use of this hybrid material will endow the electrode surface with the highest sensitivity for sensing applications. The decrease in the overpotential of the oxidation of NO (curve 1), compared to the GC/**Ni(II)-3** electrode (curve 2) would endow the electrode with a better selectivity, compared to the commonly used **Ni(II)-3** modified sensors.

In good agreement with this work, it has also been proved that the dendrite-like electropolymeric **Ni(II)-2** film crystals formed on BPPG modified SWCNT enhances the electrocatalytic detection of NO (expected to be generated from sodium nitrite in acid solution by disproportionation) [139].

To give a further insight into the characterization of the sensitivity and the selectivity of molecular materials dedicated to the electrochemical sensing of NO, Porras *et al.* [140] prepared several combinations of SWCNT, **Ni(II)-3**, electropolymerized *o*-phenylenediamine (poly-(*o*-PD)), electrografted 4-nitrobenzenediazonium (poly-NB) and dip coated Nafion® layers to modify the surface of glassy carbon (GC) electrodes. The authors compared the performances of these hybrid homemade materials, in terms of sensitivity to NO and selectivity against several interfering analytes, namely: L-arginine, ascorbate, nitrite and hydrogen peroxide. The obtained results show that GC/SWCNT-**Ni(II)-3**/poly-NB and GC/SWCNT-**Ni(II)-3**/poly-(*o*-PD)/poly-NB electrodes exhibit a good selectivity against the four examined interfering analytes. It was also noticeable that all the electrode configurations are extremely selective against L-arginine and ascorbate. In addition, GC/**Ni(II)-3**/poly-(*o*-PD), GC/**Ni(II)-3**/poly-NB and GC/SWCNT-**Ni(II)-3**/poly-(*o*-PD)/poly-NB electrodes are extremely selective against nitrite since no nitrite was detected up to 100 μM, while GC/SWCNT-**Ni(II)-3**/poly-(*o*-PD) and GC/SWCNT-**Ni(II)-3**/Nafion® hybrid materials provide poor selectivity against H_2O_2. GC/SWCNT-**Ni(II)-3**/poly-(*o*-PD)/poly-NB configuration is among the best selective material against H_2O_2. This last functionalized electrode, made of a double coating, gives promising results.

Detection of halogenated compounds

Salimi *et al*. [141] reported on **Fe(III)-16** adsorbed on MWCNTs immobilized on GC. The modified electrode exhibited excellent electrocatalytic activity toward reduction of ClO_3^-, IO_3^- and BrO_3^- in acidic solutions with detection limit in the μM range for ClO_3^-, and IO_3^-. The best sensitivity and selectivity was observed for the detection of the bromate ion with detection limit in the nM and nA/μM ranges respectively. The modified electrode showed good reproducibility, high stability, and fast amperometric response time. Nyokong and Khene have reported on the oxidation of chlorophenol [142] using **Ni(II)-6** adsorbed on SWCNT. The SWCNT and **Ni(II)-6** exhibit a mutual synergistic effect in terms of improving electrocatalysis for the detection of chlorophenols. The stability of the electrode increases in the presence of **Ni(II)-6** or **Ni(II)-1** compared to

the bare GCE. The presence of SWCNT improves the electrocatalytic response of **Ni(II)-6** but no effect is observed when NiPc was used. All modified electrodes showed improved stability towards the detection of 2,4-dichlorophenol. The best stability for the detection of chlorophenol was obtained in the presence of SWCNT with adsorbed **Ni(II)-6**.

Detection of neurotransmitters

Machado *et al*. [143] used CNTs modified with **Co(II)-1** for the detection of dopamine DA in phosphate buffer in the presence of high concentrations of ascorbic acid as an interferent agent. The peak potential for DA oxidation moves 0.39 V to less positive values compared with that of a bare GC electrode as an effect of modification CNT/**Co(II)-1**. They found a detection limit 2.56 10^{-7} M for DA detection, in the presence of ascorbic acid in concentrations up to 0.1 M. These results were obtained using differential pulse voltammetry. The same group [144] used MWCNTs modified with **Co(II)-1** in a paraffin composite electrode for the detection of epinephrine (EP) in urine. The electrochemical response of the electrode was analyzed by differential pulse voltammetry and a shift of the oxidation peak potential of 0.175 V to less positive value was observed, compared with to paraffin/graphite composite electrode without **Co(II)-1**. Experiments in PBS at pH = 6.0 were performed to determine EP without any previous step of extraction, clean-up, and derivatization, in the range from 1.33 to 5.50 μM, with a detection limit of 15.6 nM of EP in electrolyte prepared with purified water. Figure 21 shows the DPV voltammograms with the optimized parameters for various EP concentrations and the linear dependance

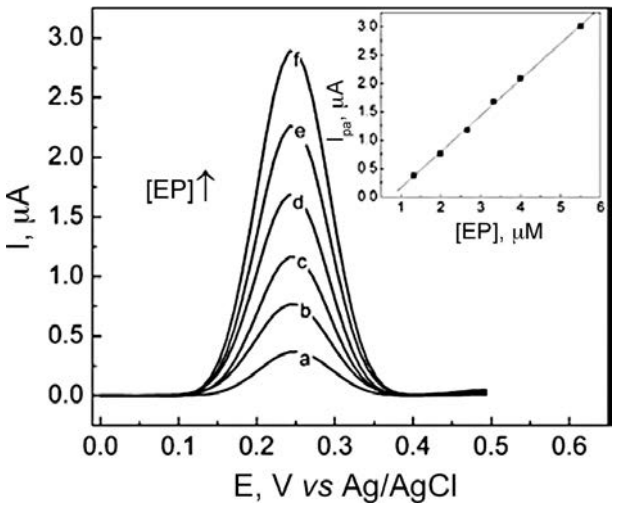

Fig. 21. Differential pulse voltammograms for paraffin/MWCNT/**Co(II)-1** composite electrode, with the optimized parameters. The epinephrine EP concentrations in M are: (a) 1.33, (b) 1.99, (c) 2.66, (d) 3.33, (e) 3.99 and (f) 5.50. Inset: linear dependence of the peak current with EP concentration; adapted from [144]

of the peak Current with EP concentration. The authors found that the lifetime of electrode was at least over 1000 determinations with 1.7 and 3.1 repeatability and reproducibility relative standard deviations, respectively. They were able to use human urine samples without any purification step under the standard addition method using paraffin/MWCNT/**Co(II)-1** composite electrode.

Other systems

Apart from the examples described above it is important to mention some other relevant molecules that are detected electrochemically using CNTs and MPc. In particular:

— MWCNT/**Co(II)-1** electrode was used for the electrochemical determination of carbaryl [145]. Figure 22A shows the square wave voltammogrammes of a bare (curve 1), GC/MWCNT (curve 2) and GC/MWCNT/**Co(II)-1** (curve 3) in 0.1 M acetate buffer (pH = 4.0) containg 0.1 mM of carbaryl. These data clearly indicate the catalytic effect induced by the hybrid material of the electrode. Figure 22B shows the square wave voltammogrammes of GC/MWCNT/**Co(II)-1** using optimized parameters to detect carbamyl at different concentration in the acetate buffer. It also shows the linear variation of the peak current with carbaryl concentrations.

— MWCNT/**Cu(II)-1** electrode was used for the detection of the herbicide glyphosate [146]. Cyclic voltammetry and electrochemical impedance spectroscopy showed that glyphosate is linked to the metallic centre of the copper phthalocyanine molecule. This analytical method was developed using differential pulsed voltammetry in pH = 7.4 phosphate buffer solution in the concentration range of 0.83–9.90 mM.

— MWCNT/**Co(II)-2** electrode was successfully reported for the oxidation of conjugated dyes [147]. The results showed that rhodamine was oxidized efficiently. In this catalytic system, MWCNTs provide strong adsorption effects to conjugated rhodamine due to their special sp2 hybridized atoms, and are able to rapidly oxidize the conjugated dye through a special electron transfer pathway.

— MWCNT, tyrosinase and **Co(II)-1** were used to prepare electrodes for the determination of bisphenol A [148]. In the composite electrode configuration, silk fibroin was used to provide a biocompatible microenvironment for the tyrosinase to retain its bioactivity. The oxidation current of bisphenol A was proportional to its concentration in the range from 5 × 10^{-8} to 3 × 10^{-6} M. The proposed method was successfully applied to determine bisphenol A in plastic products.

— Electrode containing MWCNT, CoPc and PAMAM for the detection of Avian Influenza Virus genotype was developed [149]. The DNA probes were successfully immobilized on the modified electrode with PAMAM dendrimer acting as the coupling agent.

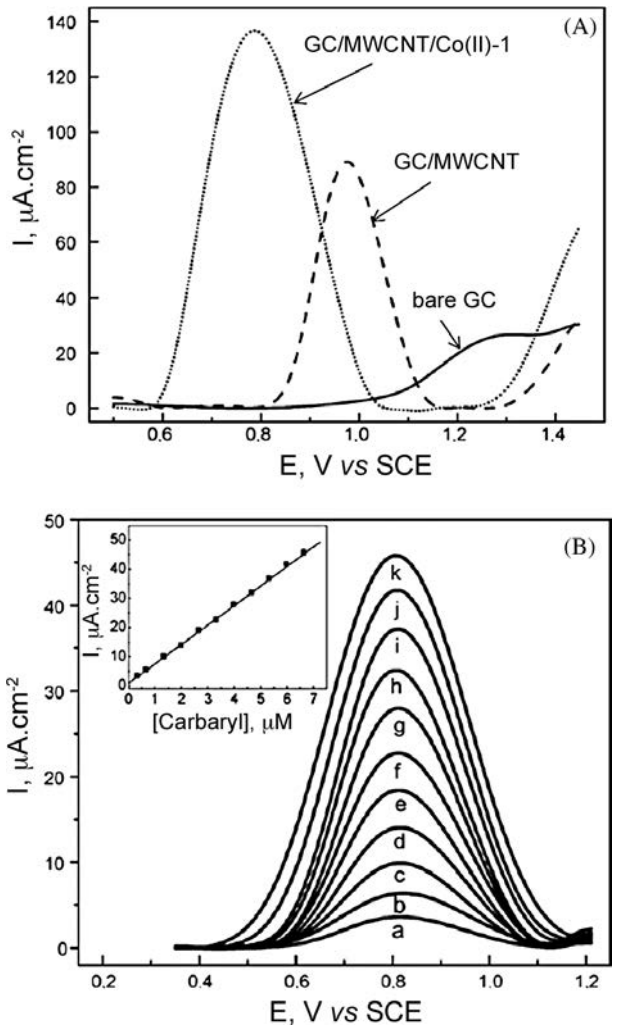

Fig. 22. (A) Square-wave voltammograms in 0.1 M acetate buffer solution (pH = 4.0), containing 1.0×10^{-4} M of carbaryl for bare GC, GC/MWCNT film and GC/MWCNT/**Co(II)-1** film electrodes. (B): Square-wave voltammograms at the GC/MWCNT/**Co(II)-1** film electrode, using the optimized SW parameters; carbaryl concentrations in μM: (a) 0.33, (b) 0.66, (c) 1.33, (d) 1.99, (e) 2.66, (f) 3.33 (g) 3.99, (h) 4.66, (i) 5.33, (j) 5.99 and (k) 6.62. Inset: linear dependence of peak current on carbaryl concentration; adapted from [145]

The difference in guanine oxidation signal of the probe modified glassy carbon electrode in the absence and presence of complementary target was linear with the logarithmic value of the complementary target concentration from 0.01 to 500 ng/mL and a detection limit of 1.0 pg/mL.

— Biosensor for glucose based on the electrochemiluminescence of luminol on glucose oxidase/poly-**Ni(II)-3**/MWCNT modified electrode was built [150]. The linear response range of glucose was 1.0×10^{-6} to 1.0×10^{-4} M. This method has been applied to determine the glucose concentrations in real serum samples with satisfactory results.

— Catalytic system using **Fe(III)-7** supported by attapulgite for degradation of Rhodamine B was proposed [151]. The results showed that it exhibited high activity for degradation of this analyte in the presence of hydrogen peroxide. The recycling test was also carried out to prove its reusability in catalytic application.

— Assembly of a picket fence porphyrin on nitrogen-doped multiwalled carbon nanotubes (CNx MWCNTs) *via* Fe–N coordination was prepared and characterized using several techniques [152]. It was found that the presence of the nitrogen-doped CNx MWCNTs led to the direct formation of a high-valent iron(IV)-porphyrin unit, that presented high catalytic activity for the oxidation of sulfite. The electrode exhibited a linear response in a range of four orders of magnitude from 8.0×10^{-7} to 4.9×10^{-3} M and a detection limit of 3.5×10^{-7} M. The electrode showed good analytical performance and could have potential applications in the detection of sulfite ions in beverages.

— Phenylamine-functionalised SWCNTs (SWCNT-phenylamine) with **Co(II)-22** was tested as hybrid electrode material for the detection of nicotinamide adenine dinucleotide (NADH) as a model of biological analyte [153]. The overpotential for the oxidation of NADH for the hybrid electrode was reduced by 0.3 V compared to the bare electrode.

— Basal plane pyrolytic graphite electrodes (BPPGEs) modified with single-wall carbon nanotube (BPPGE-SWCNT) and SWCNTs functionalised with **Co(II)-2** showed electrocatalytic responses for the detection of V-type nerve agent sulfhydryl hydrolysis products, dimethylaminoethanethiol (DMAET) and diethylaminoethanethiol (DEAET) [154]. Detection limits of approximately 8.0 and 3.0 μM for DMAET and DEAET were found with sensitivities of 5.0 and 6.0×10^{-2} AM^{-1} for DMAET and DEAET, respectively. The BPPGE-SWCNT-**Co(II)-2** hybrid electrode exhibited better potential discrimination for the detection of the sulfhydryl analytes compared to BPPGE-SWCNT.

— Hybrid electrode containing nanostructured **Ni(II)-1**/MWCNTs composite supported on a basal plane pyrolytic electrode that can have applications for the electrocatalytic detection of the pesticide asulam in phosphate-buffered solution (pH 7.0) was prepared [155]. It showed fast electron transport and high electrocatalytic activity for the oxidation of asulam, with an onset potential of *ca*. 0.150 V lower than observed for the electrode without MWCNTs or bare BPPGE. Further, the hybrid electrode is easy to fabricate and it showed good analytical performance for asulam, with a detection limit of 0.285 μM, and a linear response in the concentration range of 91–412 μM, and a sensitivity of 44.6 $\mu A.mM^{-1}$. This electrode is very attractive as a nanocomposite platform for the electrochemical detection of this pesticide.

Table 1 is restating the list of the significant examples considered in this review.

Table 1. Summary of the main N_4 complexes discussed in this review

Complex	Identification number	Central metal	References
Metallophthalocyanine	**1**	Fe(III) Co(II) Cu(II)	87, 94, 99, 106, 107, 109, 110, 119, 136, 143, 144 145, 148, 149 146
Tetra-amino metallophthalocyanine	**2**	Mn(III) Co(II) Ni(II)	80 85, 86, 90, 91, 92, 147 81, 125, 140
Tetrasulfonated metallophthalocyanine	**3**	Cu(II) Co(II) Ni(II)	83 84, 111, 112, 121 94, 140, 150
Tetra-tert-butyl metallophthalocyanine	**4**	Co(II)	107
Tetra-tert-butylphthalocyanine	**5**	—	86
Octadecyl metallophthalocyanine	**6**	Ni(II)	142, 155
Octacarboxylic acid metallophthalocyanine	**7**	Fe(III)	151
Octabutylsulphonyl metallophthalocyanine	**8**	Co(II) Fe(III)	93 93
2,9,16-trilauryloxy-23-hexyloxy metallophthalocyanine	**9**	Cu(II)	79
Tris[9(10),16(17),23(24)-(4-2-mercaptopyridine)-2-(4-carboxyphenoxy] metallophthalocyanine	**10**	Zn(II)	82
Alcian blue pyridine variant	**11**	Cu(II)	83
Tetrakis (diaquaplatinum)octacarboxy metallophthalocyanine	**12**	Fe(II) Ru(II)	100 103
Porphyrin	**13**	—	15, 85, 88
Metalloporphyrin	**14**	Mn, Fe(III), Co(II)	101, 152
Protoporphyrin IX	**15**	Fe(III) Zn(II)	85, 105, 108 89
Tetraphenyl metalloporphyrin	**16**	Fe(III)	85, 141
Tetra-(N-methyl-4-pyridyl) metalloporphyrin	**17**	Co(II) Fe(III)	99 120, 121
Tetratolyl metalloporphyrin	**18**	Mn(III) Fe(III) Co(II)	102 102 102
2,3,7,8,12,13,17,18-octaethyl-porphyrin	**19**	Co(II)	107
5,10,15,20-tetrakis(4-*tert*-butylphenyl)-metalloporphyrin	**20**	Co(II)	107
Vitamin B12	**21**	Co(II)	137
Octa[(3,5-biscarboxylate)-phenoxy]phthalocyanine	**22**	Co(II)	153

CONCLUSION

The review of the literature clearly shows that hybrid materials containing CNTs and metallophthalocyanines, metallorphyrins and other MN_4 macrocyles maintain (in some cases improve) the electrocatalytic properties without any destruction of the electronic properties of carbon nanotubes but the net result is a much higher activity due mainly to a larger dispersion of the metal complexes when they are incorporated on the carbon nanotubes. Methods of modification of CNTs using the macrocycles include non-covalent adsorption *via* π–π interactions, electropolymerisation and self-assembly. The modified CNTs have been characterized by a variety of techniques including CV, TEM, XPS, Raman and AFM. Both the phthalocyanine and porphyrin modified

SWCNTs and MWCNTs show good electrocatalytic activity towards a number of analytes such as oxygen and hydrogen peroxide reduction, oxidation of thiols and nitric oxide. Detection limits and sensitivity of the CNTs are improved when modified with the MN_4 macrocycles. It is clear that up to now the synergic effect between CNTs and MPc or MP is still not fully understood and significant amount of additional work is needed to clarify the electronic properties of these hybrid material and accurately establish a neat correlation between theses properties and the electrocatalytic behaviour.

Acknowledgements

Financial support from CNRS-CONICYT (PICS France/Chile no. 5738 (2011–2013)) and Bilateral projet CNRS-CONACYT (France/Mexico) for travel expenses is acknowledged. We are thankful to Fondecyt Project 1100773, Nucleo Milenio de Ingenieria Molecular P07-006 of Chile and Project 000153/11 of the University of Guanajuato, Mexico. M.S-N is grateful to Conicyt for a Doctoral fellowship.

REFERENCES

1. Radushkevich LV and Lukyanovich VM. *Soviet J. Phys. Chem*. 1952; **6**: 88–95.
2. Wiles PG and Abrahamson J. *Carbon* 1978; **16**: 341–349.
3. Iijima S. *Nature.* 1991; **354**: 56–58.
4. Monthioux M and Kuznetsov V. *Carbon.* 2006; **44**: 1621–1623.
5. Dai H. *Acc. Chem. Res.* 2002; **35**: 1035–1044.
6. Yakabson BI and Smally RE, *Am. Sci.* 1997; **85**: 324–336.
7. Inagaki M, Kaneko K and Nishizawa T. *Carbon*. 2004; **42**: 1401–1417.
8. Avouris P and Chen J. *Mater. Today*. 2006; **9**: 46–54.
9. Bandaru PR. *J Nanosci. Nanotech.* 2007; **7**: 1239–1267.
10. Chen Y, Lin Y, Liu Y, Doyle J, He N, Zhuang XD, Bai JR and Blau WJ. *J. Nanosci. Nanotech*. 2007; **7**: 1268–1283.
11. Lukaszewicz JP. *Sensors Lett.* 2006; **4**: 53–98.
12. Hu YH, Shenderova OA and Brenner DW. *J. Comp. Theor. Nanosci*. 2007; **4**: 199–221.
13. Guldi DM, Rahman GMA, Prato M, Jux N, Qin S and Ford W. *Angew. Chem. Int. Ed.* 2005; **44**: 2015–2018.
14. Harris PJF. *Carbon Nanotubes and Related Structures*, 1st edition, Cambridge University Press, Cambridge, UK. 1999.
15. Langa F, Gómez-Escanilla MJ and de la Cruz P. *J. Porph. Phthal*. 2007; **11**: 348–358.
16. Guo X, Huang L, O'Brien S, Kim P and Nuckolls C. *J. Am. Chem. Soc.* 2005; **127**: 15045–15047.
17. Wang J. *Electroanalysis.* 2005; **17**: 7–14.
18. Lin J, Koehne JE, Casell AM, Chen H, Ng HT, Ye Q, Fan W, Han J and Meyyappan M. *Electroanalysis* 2005; **17**: 15–27.
19. Poirier E, Chahine R, Bénard P, Cossement D, Lafi L, Mélançon E, Bose TK and Désilets S. *Appl. Phys. Mater. Sci. Process* 2004; **78:** 961–967.
20. Dehouche Z, Lafi L, Grimard N, Goyette J and Chabine R. *Nanotechnology* 2005; **16**: 402–409.
21. Villers D, Jacque-Bedard X and Dodelet JP. *J. Electrochem. Soc.* 2004; **151**: A1507–A1515.
22. Wang J, Yin G, Shao Y, Wang Z and Yunzhi G. *J. Electrochem. Soc.* 2007; **154**: B687-B693.
23. Kim YT and Mitani T. *J. Catalysis* 2006; **238**: 394–401.
24. Lee K, Zhang J, Wang H and Wilkinson DP. *J. App. Electrochem*. 2006; **36**: 507–522.
25. Sun X, Li R, Villers D, Dodelet JP and Desilets S. *Chem. Phys. Lett*. 2003; **379**: 99–104.
26. Wang X, Waje M and Yan Y. *Electrochem. Solid State Lett.* 2005; **8**: A42–A44.
27. Sun CL, Chen LC, Su MC, Hong LS, Chyan O, Hsu CY, Chen KH, Chang TF and Chang L. *Chem. Mater.* 2005; **17**: 3749–3753.
28. Villers D, Sun SH, Serventi AM, Dodelet JP and Desilets S. *J. Phys. Chem. B.* 2006; **110**: 25916–25925.
29. Dicks AL. *J. Power Source* 2006; **156**: 128–141.
30. Fakioglu E, Yurum Y and Verizoglu TN. *Intl. J. Hydrogen Storage* 2004; **29**: 1371–1376.
31. Liu HS, Song CJ, Zhang L, Zhang JJ, Wang HJ and Wilkinson DP. *J. Power Source* 2006; **155**: 95–110.
32. Mao SS and Chen XB. *Intl. J. Energ. Res*. 2007; **31**: 619–636.
33. Pandolfo AG and Hollenkamp AF. *J. Power Sources.* 2006; **157**: 11–27.
34. Wee JH, Lee KY and Kim SH. *J. Power Sources.* 2007; **165**: 667–677.
35. Zhou L. *Renew. Sust. Energ. Rev*. 2005; **9**: 395–408.
36. Tang ZK, Zhang L, Wang N, Zhang XX, Wen GH, Li GD, Wang JN, Chan CT and Sheng P. *Science*. 2001; **292**: 2462–2465.
37. http://www.sciencedaily.com /releases/1999/05/990521055614.htm.
38. Merkoçi A. *Microchim. Acta* 2005; **152**: 157–174.
39. Wang J and Musameh M. *Anal. Chim. Acta* 2004; **511**: 33–36.
40. Daniel S, Rao TP, Rao KS, Rani SU, Naidu GRK, Lee HY and Kawai T. *Sensors Actuators B* 2007; **122**: 672–682.
41. Sherigara BS, Kutner W and D'Souza F. *Electroanalysis* 2003; **15**: 753–772.
42. Salimi A, Hallaj R and Khayatian GR. *Electroanalysis* 2005; **17**: 873–879.
43. Lu G, Jiang L, Song F, Liu C and Jiang L. *Electroanalysis* 2005; **17**: 901–905.
44. Banks CE, Crossley A, Salter C, Wilkins SJ and Compton RG. *Angew. Chem. Int. Ed.* 2006; **45**: 2533–2537.

45. Banks CE and Compton RG. *Analyst.* 2006; **131**: 15–21.
46. Ji X, Kadara RO, Chen O and Banks CE. *Electroanalysis* 2010; **22**: 7–19.
47. Pillay J and Ozoemena KI. *Electrochem. Commun*. 2007; **9**: 1816–1823.
48. Britto PJ, Santhanam KSV and Ajayan PM. *Bioelectrochem. Bioenerg.* 1996; **41**: 121–125.
49. Salimi A, Noorbakhsh A and Ghadermarz M. *Anal. Biochem*. 2005; **344**: 16–24.
50. Salimi A, Compton RG and Hallaj R. *Anal. Biochem*. 2004; **333**: 49–56.
51. Salimi A and Hallaj R. *Talanta.* 2005; **66**: 967–975.
52. Liu J, Rinzler AJ, Dai H, Hafner JH, Kelley RB, Boul PJ, Lu A and Smalley RE. *Science.* 1998; **280**: 1253–1256.
53. Dillon AC, Gennett T, Jones KM, Alleman JL, Parilla PA and Heben MJ. *Adv. Mater*. 1999; **11**: 1354–1358.
54. Zhao GC, Zhang L, Wei XW and Yang ZS. *Electrochem. Commun*. 2003; **5**: 825–829.
55. Wang J, Li M, Shi Z, Li N and Gu Z. *Anal. Chem*. 2002; **74**: 1993–1997.
56. Yu X, Chattopadhyay D, Galeska I, Papadimitrakopoulos F and Rusling JF. *Electrochem. Commun.* 2003; **5**: 408–411.
57. Du P, Liu SN, Wu P and Cai CX. *Electrochim. Acta* 2007; **52**: 6534–6547.
58. Maruccio G, Visconti P, Biasco A, Bramanti A, Della Torre A, Pompa PP, Frascerra V, Arima V, D'Amone E, Cingolani R and Rinaldi R. *Electroanalysis* 2004; **16**: 1853–1862.
59. Pumera M, Sanchez S, Ichinose I and Tang J. *Sensors Actuators* B 2007; **123**: 1195–1205.
60. Wanekaya AK, Chen W, Myung NV and Mulchandani A. *Electroanalysis* 2006; **18**: 533–550.
61. Zheng W and Zheng YF. *Electrochem. Commun.* 2007; **9**: 1619–1623.
62. Yan XB, Chen XJ, Tai BK and Khor KA. *Electrochem. Commun*. 2007; **9**: 1269–1275.
63. Chakraborty S and Raj CR. *Electrochem. Commun*. 2007; **9**: 1323–1330.
64. Ivnitski D, Atanassov P and Apblett C. *Electroanalysis* 2007; **19**: 1562–1568.
65. Wu BY, Hou SH, Yin F, Zhao ZX, Wang YY, Wang XS and Chen Q. *Biosens. Bioelectron*. 2007; **22**: 2854–2860.
66. Kumar SA and Chen SM. *Biosens. Bioelectron*. 2007; **22**: 3042–3050.
67. Hu P, Tanii T, Zhang GJ, Hosaka T and Ohdomori I. *Sensors Actuators B* 2007; **124**: 161–166.
68. Yu X, Kim SN, Papadimitrakopoulos F and Rusling JF. *Mol. BioSyst.* 2005; **1**: 70–78.
69. Liu Y, Yan YL, Lei J, Wu F and Ju H. *Electrochem. Commun*. 2007; **9**: 2564–2570.
70. Zagal JH, Griveau S, Silva JF, Nyokong T and Bedioui F. *Coord. Chem. Rev*. 2010; **254**: 2755–2791.
71. Lever ABP. *J. Porph. Phthal*. 1999; **3**: 488–499.
72. Zagal JH, Bedioui F and Dodelet JP. (Eds.) *N_4-Macrocyclic Metal Complexes, Springer*, New York, 2006.
73. Bedioui F, Griveau S, Nyokong T, Appleby AJ, Caro CA, Gulppi M, Ochoa G and Zagal JH. *Phys. Chem. Chem. Phys.* 2007; **9**: 3383–3396.
74. Griveau S and Bedioui F, in Handbook of Porphyrin Sciences, eds. Kadish KM, Smith KM and Guilard R. World Scientific, San Diego. 2011; **12**: 227–296.
75. Nyokong T and Bedioui F. *J. Porph. Phthal.* 2006; **10**: 1101–1115.
76. Kadish KM, Smith KM and Guilard R. *Handbook of Porphyrin Sciences*, eds. World Scientific, San Diego. Vols. 2011; **1**: 20.
77. Leznoff CC, Lever ABP eds. *Phthalocyanines: Properties and Applications, VCH, Weinheim*. Vols. **1–4**: 1989–1993–1996.
78. Zagal JH, Griveau S, Ozoemena KI, Nyokong T and Bedioui F. *J. Nanoscience Nanotech.* 2009; **9**: 2201–2214.
79. Yang Z, Pu H, Yuan J, Wan D and Liu Y. *Chem. Phys. Lett*. 2008; **465**: 73–77.
80. Yang ZL, Chen HZ, Cao L, Li HY and Wang M. *Mater. Sci. and Eng.* 2004; **B106**: 73–78.
81. Mugadza T and Nyokong T. *Electrochim. Acta* 2010; **55**: 6049–6057.
82. Chidawanyika W and Nyokong T. *Carbon* 2010; **48**: 2831–2838.
83. Baba A, Kanetsuna Y, Sriwichai S, Ohdaira Y, Shinbo K, Kato K, Phanichphant S and Kaneko F. *Thin Solid Films* 2010; **518**: 2200–2205.
84. Agboola BO, Vilakazi SL and Ozoemena KI. *J. Solid. State Electrochem*. 2009; **13**: 1367–1379.
85. Murakami H, Nakamura G, Nomura T, Miyamoto T and Nakashima N. *J. Porph. Phthal.* 2007; **11**: 418–427.
86. Wang X, Liu Y, Qiu W and Zhu D. *J. Mat. Chem.* 2002; **12**: 1636–1639.
87. Ye JS, Wen Y, Zhang WD, Cui HF, Xu GQ and Sheu FS. *Electroanalysis* 2005; **17**: 89–96.
88. Hasobe T, Fukuzumi S and Kamat PV. *J. Am. Chem. Soc*. 2005; **127**: 11884–11885.
89. Murakami H, Nomura T and Nakashima N. *Chem. Phys. Lett*. 2003; **378**: 481–485.
90. Siswana MP, Ozoemena KI and Nyokong T. *Electrochim. Acta* 2006; **52**: 114–122.
91. Caro A, Bedioui F and Zagal JH. *Electrochim. Acta* 2002; **47**: 1489–1494.
92. Ozoemena KI, Pillay J and Nyokong T. *Electrochem. Commun*. 2006; **8**: 1391–1396.
93. Mamuru SA, Ozoemena KI, Fukuda T, Kobayashi N and Nyokong T. *Electrochimica Acta* 2010; **55**: 6367–6375.
94. Silva JF, Griveau S, Richard C, Zagal JH and Bedioui F. *Electrochem. Commun*. 2007; **9**: 1629–1634.
95. Zagal JH. *Coord. Chem. Revs.* 1992; **119**: 89–136.

96. Zagal JH, Páez M, Tanaka AA, dos Santos JR and Linkous C. *J. Electroanal. Chem*. 1992; **339**: 13–30.
97. Morcos I and Yeager E. *Electrochim. Acta* 1970; **15**: 953–975.
98. Lai ME and Bergel A. *J. Electroanal. Chem*. 2001; **494**: 30–40.
99. Qu J, Shen Y, Qu X and Dong S. *Chem. Commun*. 2004; 34–35.
100. Mamuru SA and Ozoemena KI. *Electrochem. Commun.* 2010; **12**: 1539–1542.
101. Okunola A, Kowalewska B, Bron M, Kulesza PJ and Schuhmann W. *Electrochim. Acta*. 2009; **54**: 1954–1960.
102. Okunola AO, Chikka T, Chen NX, Eckhard K and Schuhmann W. *Electrochim. Acta* 2009; **54**: 4971–4978.
103. Maxakato NW, Mamuru SA and Ozoemena KI. *Electroanalysis* 2011; **23**: 325–329.
104. Cheng F, Zhang S, Adronov A, Echegoyen L and Diederich F. *Chem. Eur. J*. 2006; **12**: 6062–6070.
105. Ye JS, Wen Y, De Zhang W, Cui HF, Gan LM, Xu GQ and Sheu FS. *J. Electroanal. Chem*. 2004; **562**: 241–246.
106. Maldonado S and Stevenson KJ, *J. Phys. Chem. B* 2004; **108**: 11375–11383.
107. Morozan A, Campidelli S, Filoramo A, Jousselme B and Palacin S. *Carbon* 2011; **49**: 4839–4847.
108. Turdean GL, Popescu IC, Curulli A and Palleschi G, *Electrochim. Acta.* 2006; **51**: 6435–6441.
109. Pillay J and Ozoemena KI. *Electrochimic. Acta* 2009; **54**: 5053–5059.
110. Lin CY, Balamurugan A, Lai YH and Ho KC. *Talanta* 2010; **82**: 1905–1911.
111 Zagal JH, Fierro C and Rozas R. *J. Electroanal. Chem*. 1981;**119**: 403–408.
112. Zagal JH and Herrera P. *Electrochim. Acta*, 1985 **30**: 449–454.
113. Sehlotho N, Nyokong T, Zagal JH and Bedioui F. *Electrochim. Acta* 2006 **51**: 5125–5130.
114. Zagal JH, Gulppi MA, Depretz and Lelièvre D, *J. Porph. Phthal*., 1999; **3**: 355–363.
115. Zagal JH, Gulppi MA, Caro CA and Cárdenas-Jirón GI, *Electrochem. Commun*. 1999; **1**: 389–393.
116. Griveau S, Pavez J, Zagal JH and Bedioui F. *J. Electroanal. Chem.* 2001; **497**: 75–83.
117. Aguirre MA, Isaacs I, Armijo F, Basáez L and Zagal JH. *Electroanalysis* 2002; **14**: 356–362.
118. Claußen JA, Ochoa G, Paez M, Costamagna J, Nyokong T, Bedioui F and Zagal JH, *J. Sol. State. Electrochem*. 2008; 12 473–481.
119. Porras Gutierrez AG, Gutierrez Granados S, Alatorre Ordaz A, Richard C, Griveau S, Zagal JH and Bedioui F. *ECS Transactions*, 2008; **15**: 133–141.
120. Luz RC, Damos FS, Tanaka AA, Kubota LT and Gushikem Y. *Talanta* 2008; **76**: 1097–1104.
121. Luz RCS, Maroneze CM, Tanaka AA, Kubota LT, Gushikem Y and Damos FS. *Microchim. Acta*. 2010; **171**: 169–178.
122. Zagal J, *J. Electroanal. Chem*. 1980; **109**: 389–393.
123. Zagal J, Muñoz E and Ureta-Zañartu S. *Electrochim. Acta* 1982; **27**: 1373–1377.
124. Zagal J and Ureta-Zañartu S. *J. Electrochem. Soc.*, 1982; **129**: 2249–2247.
125. Korfhage KM, Ravichandran K and Baldwin RP. *Anal. Chem*. 1984; **56**: 1514–1517.
126. Halbert MK and Baldwin RP. *Anal. Chem.* 1985; **57**: 591–595.
127. Zagal J, Lira S and Ureta-Zañartu S. *J. Electroanal. Chem.*, 1986; **210**: 95–110.
128. Zagal JH and Páez MA. *Electrochim. Acta*., 1997; **42**: 3477–3481.
129. Isaacs I, Aguirre MJ, Toro-Labbé A, Costamagna J, Paez M and Zagal JH. *Electrochim. Acta*., 1998; **43**: 1821–1827.
130. Geraldo D, Linares C, Chen Y-Y, Ureta-Zañartu S and Zagal JH. *Electrochem. Comm.* 2002; **4**: 182–188.
131. Linares C, Geraldo D, Paez M and Zagal JH. *J. Solid. State Electrochem*. 2003; **7**: 626–632.
132. Venegas-Yazigi D, Cárdenas-Jirón GI and Zagal JH. *J. Coord. Chem.* 2003; **56**: 1269–1275.
133. Paredes-García V, Cárdenas-Jirón GI, Venegas-Yazigi D, Zagal JH, Páez M and Costamagna J. *J. Phys. Chem. A* 2005; **109**: 1196–1204.
134. Cárdenas-Jirón GI, Paredes-García V, Venegas-Yazigi D, Zagal JH, Páez M and Costamagna JA. *J. Phys. Chem. A*, 2006; **110**: 11870–11875.
135. Trollund E, Ardiles P, Aguirre MJ, Biaggio SR and Rocha Filho RC. *Polyhedron*, 2000; **19**: 2303–2312.
136. Geraldo DA, Togo CA, Limson J and Nyokong T. *Electrochim. Acta* 2008; **53**: 8051–8057.
137. Umasankar Y, Huang T and Chen S. *Anal. Biochem.* 2011; **408**: 297–303.
138. Bedioui F and Villeneuve N. *Electroanalysis* 2003; **15**: 5–18.
139. Pillay J and Ozoemena KI. *Chem. Phys. Lett.* 2007; **441**: 72–77.
140. Porras A, Griveau S, Richard C, Pailleret A, Gutierrez S and Bedioui F. *Electroanalysis* 2009; **21**: 2303–2310.
141. Salimi A, Mamkhezri H, Hallaj R and Zandi S. *Electrochim. Acta* 2007; **52**: 6097–6105.
142. Khene S and Nyokong T. *Electroanalysis*, 2011; **23**: 1901–1911.
143. Cruz Moraes F, Cabral FM, S Machado SAS and Mascaro LH, *Electroanalysis* 2008; **20**: 851–857.
144. Cruz Moraes F, Golineli D, Mascaro L and Machado SAS. *Sensors and Actuators B* 2010; **148**: 492–497.
145. Cruz Moraes F, Mascaro LH and Machado SAS and Brett CMA. *Talanta*. 2009; **79**: 1406–1411.

146. Cruz Moraes F, Mascaro LH and Machado SAS and Brett CMA. *Electroanalysis* 2010; **22**: 1586–1591.
147. Lu W, Li N, Chen W and Yao Y. *Carbon* 2009; **47**: 3337–3345.
148. Yin H, Zhou Y, Xu J, Ai S, Cui L and Zhu L. *Anal. Chim. Acta* 2010; **659**: 144–150.
149. Zhu X, Ai S, Chen Q, Yin H and Xu J. *Electrochem. Commun.* 2009; **11**: 1543–1546.
150. Qiu B, Lin Z, Wang J, Chen Z, Chen J and Chen G. *Talanta* 2009; **78**: 76–80.
151. Fang Y and Chen D. *Mater. Res. Bull.* 2010; **45**: 1728–1731.
152. Tu W, Lei J, Jian G, Hu Z and Ju H. *Chem. Eur. J.* 2010; **16**: 4120–4126.
153. Agboola BO, Ozoemena KI, Nyokong T, Fukuda T and Kobayashi N. *Carbon.* 2010*;* **48**: 763–773.
154. Pillay J and Ozoemena KI. *Electrochim. Acta* 2007*;* **52**: 3630–3640.
155. Msimelelo P, Siswana MP, Ozoemena KI, Geraldo DA and Nyokong T. *J Solid State Electrochem.* 2010; **14**: 1351–1358.

